Enhancement of the phonon-sideband luminescence in semiconductor microcavities

C. N. Böttge,* M. Kira, and S. W. Koch
Department of Physics and Material Sciences Center, Philipps-University of Marburg, Renthof 5, D-35032 Marburg, Germany
(Received 14 December 2011; published 5 March 2012)

The influence of a semiconductor microcavity on the phonon-assisted photoluminescence is investigated by expanding the microscopic quantum-optical semiconductor luminescence equations. For the example of a ZnO-based system, strong enhancement but no normal-mode splitting of the phonon-sideband luminescence is predicted, even if the cavity becomes resonant with the first phonon sideband. For increasing cavity quality, it is shown that the intensity of the 1*s* resonance first increases due to the Purcell effect but then starts to decrease due to the transition into the nonperturbative regime, while the spectral integrated phonon-sideband intensity saturates.

DOI: 10.1103/PhysRevB.85.094301 PACS number(s): 71.38.−k, 78.55.Cr, 42.79.Gn

I. INTRODUCTION

Zinc oxide (ZnO) exhibits a wide range of interesting properties. For example, its wide band gap that allows optical transitions in the blue/ultraviolet range could become important for semiconductor laser applications.[1,2] In optical experiments on ZnO, both the Coulomb and the electron–phonon interaction influence the resulting spectra. First of all, ZnO has a very large excitonic binding energy of about 60 meV,[3–5] which leads to strong excitonic signatures in the absorption and photoluminescence even at room temperature.[6–8] Moreover, due to its highly polar nature, the strong interaction between electrons and longitudinal-optical (LO) phonons in ZnO gives rise to pronounced phonon sidebands in the luminescence spectra.[4,8–16] Since the LO phonons have a discrete energy, phonon-assisted processes can create multiple replicas, i.e., phonon sidebands (PSBs) at distinct frequencies below the original excitonic resonance.[11,14,17] Traditionally, the excitonic resonance is called the zero-phonon line (ZPL).[12,15,18–21]

The emission properties of a quantum well (QW) can be strongly modified by its radiative environment, e.g., yielding the Purcell effect,[22] inhibited emission,[23] or the scenario of normal-mode coupling (NMC),[24–26] where the eigenmode of a high-quality microcavity and the exciton resonance are strongly coupled. Typically, such a microcavity is realized by growing distributed Bragg reflectors (DBRs) as mirrors around the QWs. For systems with strong PSBs, it is clearly interesting to study what happens to a PSB when it is coupled with a cavity mode. In ZnO, the first PSB lies 72 meV below the ZPL resonance, producing clearly separated PSB and ZPL features, which makes ZnO an attractive candidate for such investigations.

In this paper, we study how PSB luminescence is altered by an optical cavity. To develop a consistent microscopic theory of the sideband emission, we generalize the semiconductor luminescence equations (SLEs)[27–29] by fully including phonon-assisted processes. As an extension of our earlier work,[11,17] this approach allows us to compute both spontaneous and stimulated emission at the excitonic resonance and its first sideband. To corroborate our numerical results, we develop an analytic model to describe the main features of phonon-assisted luminescence in a cavity.

This paper is structured as follows. Section II presents the system Hamiltonian and Sec. III discusses the equations of motion used for the numerical and analytic calculations. Section IV reveals the principal effects of a dielectric environment. The analytic model is developed in Sec. V where the equations of motion are solved in a steady state. The appendices contain additional details of the exciton basis used and of the analytic model.

II. SYSTEM HAMILTONIAN

In our microscopic description of the optical properties, we start from the generic semiconductor Hamiltonian[27,29,30] for a two-band QW:

$$\begin{aligned} H = &\sum_{\lambda,\mathbf{k}} \epsilon^{\lambda}_{\mathbf{k}}\, a^{\dagger}_{\lambda,\mathbf{k}} a_{\lambda,\mathbf{k}} + \sum_{\mathbf{q}_{3D}} \hbar\omega_{\mathbf{q}_{3D}} \left(B^{\dagger}_{\mathbf{q}_{3D}} B_{\mathbf{q}_{3D}} + \frac{1}{2} \right) \\ &+ \sum_{\mathbf{p}_{3D}} \hbar\Omega_{\mathbf{p}_{3D}} \left(D^{\dagger}_{\mathbf{p}_{3D}} D_{\mathbf{p}_{3D}} + \frac{1}{2} \right) \\ &+ \frac{1}{2} \sum_{\lambda,\lambda'} \sum_{\mathbf{k},\mathbf{k}',\mathbf{q}\neq 0} V_{\mathbf{q}}\, a^{\dagger}_{\lambda,\mathbf{k}} a^{\dagger}_{\lambda',\mathbf{k}'} a_{\lambda',\mathbf{k}'+\mathbf{q}} a_{\lambda,\mathbf{k}-\mathbf{q}} \\ &+ \sum_{\lambda,\mathbf{k},\mathbf{p}_{3D}} \hbar\Omega_{\mathbf{p}_{3D}}\, g^{\lambda}_{\mathbf{p}_{3D}} a^{\dagger}_{\lambda,\mathbf{k}-\mathbf{p}} a_{\lambda,\mathbf{k}} \left(D_{-\mathbf{p}_{3D}} + D^{\dagger}_{\mathbf{p}_{3D}} \right) \\ &- \sum_{\mathbf{k},\mathbf{q}_{3D}} \mathrm{i} \left(\mathcal{F}_{\mathbf{q}_{3D}} a^{\dagger}_{\mathrm{c},\mathbf{k}+\mathbf{q}} a_{\mathrm{v},\mathbf{k}} + \mathcal{F}^{\star}_{\mathbf{q}_{3D}} a^{\dagger}_{\mathrm{v},\mathbf{k}} a_{\mathrm{c},\mathbf{k}-\mathbf{q}} \right) B_{\mathbf{q}_{3D}} + \mathrm{H.c.} \end{aligned} \tag{1}$$

Here, the electrons are described via the Fermionic operators $a^{\dagger}_{\lambda,\mathbf{k}}$ and $a_{\lambda,\mathbf{k}}$. The noninteracting parts contain the single-particle energy $\epsilon^{\lambda}_{\mathbf{k}}$ for an electron with momentum $\hbar\mathbf{k}$ in band λ, the photon energy $\hbar\omega_{\mathbf{q}_{3D}}$, and the phonon energy $\hbar\Omega_{\mathbf{p}_{3D}}$. We assume a sufficiently strong carrier confinement such that we only need to consider one conduction and valence band. We also use parabolic approximation $\epsilon^{\lambda}_{\mathbf{k}} = \frac{\hbar^2\mathbf{k}^2}{2m_{\lambda}}$ with the effective mass m_{λ} to describe excitations near the bottom of the bands. Since we are interested in longitudinal-optical phonons, with a constant dispersion relation, we set the phonon energy to a constant value of $\Omega_{\mathbf{p}_{3D}} \equiv \Omega$.

We consider here ZnO QWs where carriers are confined in the x-y plane. In this situation, it is beneficial to decompose the photon and phonon wave vectors into in-plane and z components, using $\mathbf{q}_{3D} = (\mathbf{q}, q_{\perp})$ and $\mathbf{p}_{3D} = (\mathbf{p}, p_{\perp})$. The corresponding subsystems are described by the Bosonic

creation (annihilation) operators $D^{\dagger}_{\mathbf{p}_{3D}}$ ($D_{\mathbf{p}_{3D}}$) for the phonons and $B^{\dagger}_{\mathbf{q}_{3D}}$ ($B_{\mathbf{q}_{3D}}$) for the photons. The remaining terms within H define the interactions of the carrier–photon–phonon system. More specifically, $V_{\mathbf{q}}$ is the Coulomb-matrix element, $\mathcal{F}_{\mathbf{q}_{3D}}$ defines the strength of the light-matter interaction, and $g^{\lambda}_{\mathbf{p}_{3D}}$ yields the carrier–phonon coupling. From those, $\mathcal{F}_{\mathbf{q}_{3D}} \equiv \mathscr{E}_{\mathbf{q}_{3D}} \mathbf{u}_{\mathbf{q}_{3D}} \cdot \mathbf{d}_{cv}$ contains the vacuum-field amplitude $\mathscr{E}_{\mathbf{q}_{3D}}$,[27] light mode strength $\mathbf{u}_{\mathbf{q}_{3D}}(r_{\perp})$ at the QW position, and the dipole-matrix element $\mathbf{d}_{cv}$ for optical interband transitions in ZnO.

III. THEORY OF PHONON-SIDEBAND LUMINESCENCE

Due to the Coulomb- and quantum-optical interaction in Eq. (1), the operator dynamics yields the well-known hierarchy problem,[30] producing an infinite number of coupled equations. We truncate this hierarchy systematically using the so-called cluster-expansion approach[29,31–35] to the correlation dynamics. This approach expresses N-particle expectation values consistently in terms of all possible factorizations into single-particle quantities (singlets), two-particle correlations (doublets), three-particle correlations (triplets), and so on, up to correlated N-particle clusters. For example, a singlet level produces the semiconductor Bloch equations[30] that connect the classical light $\langle B_{\mathbf{q}} \rangle$ with polarization $P_{\mathbf{k}} = \langle a^{\dagger}_{\mathrm{v},\mathbf{k}} a_{\mathrm{c},\mathbf{k}} \rangle$ and densities $f^{\mathrm{e}}_{\mathbf{k}} = \langle a^{\dagger}_{\mathrm{c},\mathbf{k}} a_{\mathrm{c},\mathbf{k}} \rangle$ and $f^{\mathrm{h}}_{\mathbf{k}} = \langle a^{\dagger}_{\mathrm{v},\mathbf{k}} a_{\mathrm{v},\mathbf{k}} \rangle$.

For incoherent conditions, $\langle B_{\mathbf{q}} \rangle$ and $P_{\mathbf{k}}$ vanish. Therefore, incoherent light emission stems from doublet correlations, $\Delta\langle B^{\dagger} B \rangle = \langle B^{\dagger} B \rangle - \langle B^{\dagger} \rangle \langle B \rangle$, or higher-order correlations. We concentrate next exclusively on the incoherent regime where the photon number and its correlation are equal, i.e., $\Delta\langle B^{\dagger} B \rangle = \langle B^{\dagger} B \rangle$, because a singlet $\langle B \rangle$ vanishes. For the phonon-sideband analysis, we need to include contributions up to three-particle correlations to produce a closed set of equations describing the system consistently.

A. Semiconductor luminescence equations

The incoherent light emission follows from photon-number-like correlations,

$$\mathrm{i}\hbar \frac{\partial}{\partial t} \Delta\langle B^{\dagger}_{\mathbf{q}_{3D}} B_{\mathbf{q},q'_{\perp}} \rangle = \big(\hbar\omega_{\mathbf{q},q'_{\perp}} - \hbar\omega_{\mathbf{q}_{3D}}\big) \Delta\langle B^{\dagger}_{\mathbf{q}_{3D}} B_{\mathbf{q},q'_{\perp}} \rangle + \mathrm{i} \sum_{\mathbf{k}} \big[\mathcal{F}^{\star}_{\mathbf{q},q'_{\perp}} \Pi_{\mathbf{k},\mathbf{q}_{3D}} + \mathcal{F}_{\mathbf{q}_{3D}} \Pi^{\star}_{\mathbf{k},\mathbf{q},q'_{\perp}} \big], \tag{2}$$

which are coupled to photon-assisted polarizations $\Pi_{\mathbf{k},\mathbf{q}_{3D}} \equiv \Delta\langle B^{\dagger}_{\mathbf{q}_{3D}} a^{\dagger}_{\mathrm{v},\mathbf{k}-\mathbf{q}_{\mathrm{h}}} a_{\mathrm{c},\mathbf{k}+\mathbf{q}_{\mathrm{e}}} \rangle$ where the photon momentum $\mathbf{q}$ is divided among the electron and hole according to $\mathbf{q}_{\mathrm{e}} = \frac{m_{\mathrm{e}}}{m_{\mathrm{e}}+m_{\mathrm{h}}}\mathbf{q}$ and $\mathbf{q}_{\mathrm{h}} = \frac{m_{\mathrm{h}}}{m_{\mathrm{e}}+m_{\mathrm{h}}}\mathbf{q}$. This defines the photon flux

$$I_{\mathrm{PL}}\big(\omega_{\mathbf{q}_{3D}}\big) = \frac{\partial}{\partial t} \Delta\langle B^{\dagger}_{\mathbf{q}_{3D}} B_{\mathbf{q}_{3D}} \rangle = \mathrm{Re}\left[\sum_{\mathbf{k}} \mathcal{F}^{\star}_{\mathbf{q}_{3D}} \Pi_{\mathbf{k},\mathbf{q}_{3D}} \right], \tag{3}$$

which is proportional to the photoluminescence spectrum for quasistationary emission.[27] The corresponding equation of motion for the photon-assisted polarizations can be written as

$$\begin{aligned} \mathrm{i}\hbar \frac{\partial}{\partial t} \Pi_{\mathbf{k},\mathbf{q}_{3D}} = {} & \big(\epsilon^{\mu}_{\mathbf{k}} + \epsilon^{M}_{\mathbf{q}} - \Sigma_{\mathbf{k},\mathbf{q}} - \hbar\omega_{\mathbf{q}_{3D}}\big)\Pi_{\mathbf{k},\mathbf{q}_{3D}} \\ & - \big(1 - f^{\mathrm{e}}_{\mathbf{k}+\mathbf{q}_{\mathrm{e}}} - f^{\mathrm{h}}_{\mathbf{k}-\mathbf{q}_{\mathrm{h}}}\big) \sum_{\mathbf{k}'} V_{\mathbf{k}-\mathbf{k}'} \Pi_{\mathbf{k}',\mathbf{q}_{3D}} \\ & - (1 - f^{\mathrm{e}}_{\mathbf{k}+\mathbf{q}_{\mathrm{e}}} - f^{\mathrm{h}}_{\mathbf{k}-\mathbf{q}_{\mathrm{h}}}) \Delta\Omega_{\mathbf{q}_{3D}} + \Omega^{\mathrm{SE}}_{\mathbf{k},\mathbf{q}_{3D}} \\ & + \hbar\Omega \sum_{\mathbf{p}_{3D}} \big[g^{\mathrm{c}}_{\mathbf{p}_{3D}} \big(\Upsilon^{\mathrm{em}}_{\mathbf{k},\mathbf{q}_{3D},\mathbf{p}_{3D}} + \Upsilon^{\mathrm{abs}}_{\mathbf{k},\mathbf{q}_{3D},\mathbf{p}_{3D}} \big) \\ & - g^{\mathrm{v}}_{\mathbf{p}_{3D}} \big(\Upsilon^{\mathrm{em}}_{\mathbf{k}-\mathbf{p},\mathbf{q}_{3D},\mathbf{p}_{3D}} + \Upsilon^{\mathrm{abs}}_{\mathbf{k}-\mathbf{p},\mathbf{q}_{3D},\mathbf{p}_{3D}} \big) \big] + T[\Pi]. \end{aligned} \tag{4}$$

For parabolic bands, the sum of the single-particle energies $\epsilon^{\mathrm{e}}_{\mathbf{k}+\mathbf{q}_{\mathrm{e}}} + \epsilon^{\mathrm{h}}_{\mathbf{k}-\mathbf{q}_{\mathrm{h}}} = \epsilon^{\mu}_{\mathbf{k}} + \epsilon^{M}_{\mathbf{q}}$ can be decomposed into $\epsilon^{\mu}_{\mathbf{k}} = \frac{\hbar^2\mathbf{k}^2}{2\mu}$ and $\epsilon^{M}_{\mathbf{q}} = \frac{\hbar^2\mathbf{q}^2}{2M}$, where $\mu = (\frac{1}{m_{\mathrm{e}}} + \frac{1}{m_{\mathrm{h}}})^{-1}$ is the reduced mass and $M = m_{\mathrm{e}} + m_{\mathrm{h}}$ is the total mass. These energy terms appear in Eq. (4) together with the Coulomb renormalization,

$$\Sigma_{\mathbf{k},\mathbf{q}} \equiv \sum_{\mathbf{k}'} V_{\mathbf{k}-\mathbf{k}'} \big(f^{\mathrm{e}}_{\mathbf{k}'+\mathbf{q}_{\mathrm{e}}} + f^{\mathrm{h}}_{\mathbf{k}'-\mathbf{q}_{\mathrm{h}}} \big), \tag{5}$$

whenever carriers are excited in the system. Equations (2)–(4) constitute the principal structure of the semiconductor luminescence equations (SLEs),[27,29] where the explicit Coulomb sum yields excitonic resonances in the photoluminescence (PL). We have also included the phonon-assisted triplets

$$\Upsilon^{\mathrm{em}}_{\mathbf{k},\mathbf{q}_{3D},\mathbf{p}_{3D}} = \Delta\big\langle B^{\dagger}_{\mathbf{q}_{3D}} D^{\dagger}_{\mathbf{p}_{3D}} a^{\dagger}_{\mathrm{v},\mathbf{k}-\mathbf{Q}_{\mathrm{h}}} a_{\mathrm{c},\mathbf{k}+\mathbf{Q}_{\mathrm{e}}} \big\rangle \tag{6}$$

and

$$\Upsilon^{\mathrm{abs}}_{\mathbf{k},\mathbf{q}_{3D},\mathbf{p}_{3D}} = \Delta\big\langle B^{\dagger}_{\mathbf{q}_{3D}} D_{-\mathbf{p},\,p_{\perp}} a^{\dagger}_{\mathrm{v},\mathbf{k}-\mathbf{Q}_{\mathrm{h}}} a_{\mathrm{c},\mathbf{k}+\mathbf{Q}_{\mathrm{e}}} \big\rangle \tag{7}$$

that describe three-particle correlations due to phonon emission and absorption, respectively. Here, we introduced the center-of-mass momentum $\mathbf{Q} \equiv \mathbf{p} + \mathbf{q} = (\mathbf{p} + \mathbf{q})_{\mathrm{e}} + (\mathbf{p} + \mathbf{q})_{\mathrm{h}}$. The emerging correlations Υ generalize the SLEs to fully include phonon sidebands. The remaining triplet terms result from the Coulomb interaction. They do not directly participate in phonon-assisted processes but provide excitation-induced broadening and shifts of the emission resonances. The explicit format of the triplets $T[\Pi]$ is discussed in Ref. 29. In this paper, we treat these contributions at the level of a dephasing approximation, $T[\Pi] = -\mathrm{i}\gamma_0 \Pi_{\mathbf{k},\mathbf{q}_{3D}}$ defined by γ_0.

When a cavity is present, we must also include the stimulated feedback of light,

$$\Delta\Omega_{\mathbf{q}_{3D}} = \mathrm{i} \sum_{q'_{\perp}} \mathcal{F}_{\mathbf{q},q'_{\perp}} \Delta\big\langle B^{\dagger}_{\mathbf{q}_{3D}} B_{\mathbf{q},q'_{\perp}} \big\rangle, \tag{8}$$

that yields the coupling between the different photon modes. This contribution in particular produces the well-known normal-mode splitting of excitonic resonances in high-quality cavities, which is also a focus of this study. The spontaneous emission itself is initiated by

$$\Omega^{\mathrm{SE}}_{\mathbf{k},\mathbf{q}_{3D}} = \mathrm{i}\mathcal{F}_{\mathbf{q}_{3D}} \left(f^{\mathrm{e}}_{\mathbf{k}+\mathbf{q}_{\mathrm{e}}} f^{\mathrm{h}}_{\mathbf{k}-\mathbf{q}_{\mathrm{h}}} + \sum_{\mathbf{k}'} c^{\mathbf{q},\mathbf{k},\mathbf{k}'}_{\mathrm{X}} \right) \tag{9}$$

that is nonvanishing as soon as electrons and holes are present or when the system contains exciton correlations, $c_{\mathrm{X}}^{\mathbf{q},\mathbf{k},\mathbf{k}'} = \Delta\langle a^{\dagger}_{\mathrm{c},\,\mathbf{k}'+\mathbf{q}_{\mathrm{e}}} a^{\dagger}_{\mathrm{v},\,\mathbf{k}-\mathbf{q}_{\mathrm{h}}} a_{\mathrm{c},\,\mathbf{k}+\mathbf{q}_{\mathrm{e}}} a_{\mathrm{v},\,\mathbf{k}'-\mathbf{q}_{\mathrm{h}}}\rangle$.

Typically, the carrier distributions reach their quasiequilibrium form very rapidly via Coulomb and phonon scattering. In comparison, the spontaneous emission proceeds slowly on a nanosecond time scale such that both f^{λ} and c_{X} can be considered quasistationary when momentary PL spectra are analyzed. Therefore, we can choose them to be constant and can now concentrate on the new terms appearing in Eq. (4) to describe PSB luminescence. Technically, we must first determine Υ and then sum over all phonon momenta $\mathbf{p}$ of the phonon- and photon-assisted polarization. From these contributions, only Υ^{em} yields photon emission that is below the excitonic lines. We therefore construct the dynamics of Υ^{em} explicitly. The analysis of Υ^{abs} follows analogously; however, it is irrelevant for the PSBs studied here. The Υ^{abs} become important only if phonon absorption is relevant, requiring $k_{\mathrm{B}}T \gg \hbar\Omega$.

B. Phonon-assisted contributions

For a closed set of phonon-assisted semiconductor luminescence equations, we have to include the Υ^{em} dynamics. After deriving the Heisenberg equations of motion and taking the triplet level of the cluster expansion approach into account, we obtain

$$\begin{aligned}
\mathrm{i}\hbar\frac{\partial}{\partial t}\,\Upsilon^{\mathrm{em}}_{\mathbf{k},\mathbf{q}_{3\mathrm{D}},\mathbf{p}_{3\mathrm{D}}} &= \left(\epsilon^{\mu}_{\mathbf{k}} + \epsilon^{M}_{\mathbf{Q}} - \Sigma_{\mathbf{k},\mathbf{Q}} - \hbar\omega_{\mathbf{q},\,q_{\perp}} - \hbar\Omega\right)\Upsilon^{\mathrm{em}}_{\mathbf{k},\mathbf{q}_{3\mathrm{D}},\mathbf{p}_{3\mathrm{D}}} \\
&\quad - \left(1 - f^{\mathrm{e}}_{\mathbf{k}+\mathbf{Q}_{\mathrm{e}}} - f^{\mathrm{h}}_{\mathbf{k}-\mathbf{Q}_{\mathrm{h}}}\right)\left[\sum_{\mathbf{k}'} V_{\mathbf{k}-\mathbf{k}'}\,\Upsilon^{\mathrm{em}}_{\mathbf{k}',\mathbf{q}_{3\mathrm{D}},\mathbf{p}_{3\mathrm{D}}} + \mathrm{i}\sum_{q'_{\perp}} \mathcal{F}_{\mathbf{q}+\mathbf{p},\,q'_{\perp}}\,\Delta\left\langle D^{\dagger}_{\mathbf{p}_{3\mathrm{D}}} B^{\dagger}_{\mathbf{q}_{3\mathrm{D}}} B_{\mathbf{q}+\mathbf{p},\,q'_{\perp}}\right\rangle\right] \\
&\quad + \mathrm{i}\mathcal{F}_{\mathbf{q}_{3\mathrm{D}}}\left(f^{\mathrm{h}}_{\mathbf{k}-\mathbf{Q}_{\mathrm{h}}}\,\Xi^{\mathrm{c,\,c}}_{\mathbf{k},\mathbf{p}_{3\mathrm{D}},\mathbf{q}} - f^{\mathrm{e}}_{\mathbf{k}+\mathbf{Q}_{\mathrm{e}}}\,\Xi^{\mathrm{v,\,v}}_{\mathbf{k},\mathbf{p}_{3\mathrm{D}},\mathbf{0}} + \sum_{\mathbf{k}'}\,\Delta\left\langle D^{\dagger}_{\mathbf{p}_{3\mathrm{D}}} a^{\dagger}_{\mathrm{c},\,\mathbf{k}'-\mathbf{p}_{\mathrm{h}}} a^{\dagger}_{\mathrm{v},\,\mathbf{k}-\mathbf{Q}_{\mathrm{h}}} a_{\mathrm{c},\,\mathbf{k}+\mathbf{Q}_{\mathrm{e}}} a_{\mathrm{v},\,\mathbf{k}'-\mathbf{p}_{\mathrm{h}}-\mathbf{q}}\right\rangle\right) + Q[\Upsilon], \qquad (10)
\end{aligned}$$

where $\mathbf{Q} = \mathbf{p} + \mathbf{q}$ is again the center-of-mass momentum. The emerging quadruplets are presented only symbolically. They provide dephasing for the Υ^{em} processes, which is approximated via $Q[\Upsilon] = -\mathrm{i}\gamma_1\,\Upsilon^{\mathrm{em}}_{\mathbf{k},\mathbf{q}_{3\mathrm{D}},\mathbf{p}_{3\mathrm{D}}}$. Equation (10) shows a similar structure as Eq. (4) and is coupled to the phonon-assisted two-photon correlations,

$$\begin{aligned}
\mathrm{i}\hbar\frac{\partial}{\partial t}\Delta\left\langle D^{\dagger}_{\mathbf{p}_{3\mathrm{D}}} B^{\dagger}_{\mathbf{q}_{3\mathrm{D}}} B_{\mathbf{q}+\mathbf{p},q'_{\perp}}\right\rangle &= \left(\hbar\omega_{\mathbf{q}+\mathbf{p},q'_{\perp}} - \hbar\omega_{\mathbf{q},q_{\perp}} - \hbar\Omega\right)\Delta\left\langle D^{\dagger}_{\mathbf{p}_{3\mathrm{D}}} B^{\dagger}_{\mathbf{q}_{3\mathrm{D}}} B_{\mathbf{q}+\mathbf{p},q'_{\perp}}\right\rangle \\
&\quad + \mathrm{i}\mathcal{F}_{\mathbf{q}_{3\mathrm{D}}}\sum_{\mathbf{k}}\left[\Upsilon^{\mathrm{abs}}_{\mathbf{k},(\mathbf{q}-\mathbf{p},q'_{\perp}),(-\mathbf{p},p_{\perp})}\right]^{\star} \\
&\quad + \mathrm{i}\mathcal{F}^{\star}_{\mathbf{q}+\mathbf{p},q'_{\perp}}\sum_{\mathbf{k}}\Upsilon^{\mathrm{em}}_{\mathbf{k},\mathbf{q}_{3\mathrm{D}},\mathbf{p}_{3\mathrm{D}}} \\
&\quad + \hbar\Omega\sum_{\lambda,\mathbf{k}} g^{\lambda}_{-\mathbf{p}_{3\mathrm{D}}}\Delta\left\langle B^{\dagger}_{\mathbf{q}_{3\mathrm{D}}} B_{\mathbf{q}+\mathbf{p},q'_{\perp}} a^{\dagger}_{\lambda,\mathbf{k}+\mathbf{p}} a_{\lambda,\mathbf{k}}\right\rangle. \qquad (11)
\end{aligned}$$

The appearing $\hbar\Omega\sum g^{\lambda}\langle B^{\dagger}Ba^{\dagger}_{\lambda}a_{\lambda}\rangle$ is a pure intraband process; its contribution to the photon emission scales as $(f^{\lambda})^2$.[36] For the low densities studied here, this contribution can therefore be dropped without affecting the results. The right-hand side of Eq. (10) additionally contains the contributions $\Xi^{\lambda,\lambda}_{\mathbf{k},\mathbf{p}_{3\mathrm{D}},\mathbf{q}}$ representing phonon-assisted scattering that initiate the correlations Υ^{em}. Since these evolve quickly into quasiequilibrium, we include them via their steady-state forms

$$\Delta\left\langle D^{\dagger}_{\mathbf{p}_{3\mathrm{D}}} a^{\dagger}_{\mathrm{c},\,\mathbf{k}-\mathbf{Q}_{\mathrm{h}}+\mathbf{q}} a_{\mathrm{c},\,\mathbf{k}+\mathbf{Q}_{\mathrm{e}}}\right\rangle = \frac{\hbar\Omega\left(g^{\mathrm{c}}_{\mathbf{p}_{3\mathrm{D}}}\right)^{\star} f^{\mathrm{e}}_{\mathbf{k}+\mathbf{Q}_{\mathrm{e}}}}{\epsilon^{\mathrm{e}}_{\mathbf{k}+\mathbf{Q}_{\mathrm{e}}} - \epsilon^{\mathrm{e}}_{\mathbf{k}-\mathbf{Q}_{\mathrm{h}}+\mathbf{q}} - \hbar\Omega - \mathrm{i}\eta_{\mathrm{e}}} + O(f^2), \qquad (12)$$

$$\Delta\left\langle D^{\dagger}_{\mathbf{p}_{3\mathrm{D}}} a^{\dagger}_{\mathrm{v},\,\mathbf{k}-\mathbf{Q}_{\mathrm{h}}} a_{\mathrm{v},\,\mathbf{k}+\mathbf{Q}_{\mathrm{e}}-\mathbf{q}}\right\rangle = \frac{\hbar\Omega\left(g^{\mathrm{v}}_{\mathbf{p}_{3\mathrm{D}}}\right)^{\star} f^{\mathrm{h}}_{\mathbf{k}-\mathbf{Q}_{\mathrm{h}}}}{\epsilon^{\mathrm{h}}_{\mathbf{k}-\mathbf{Q}_{\mathrm{h}}} - \epsilon^{\mathrm{h}}_{\mathbf{k}+\mathbf{Q}_{\mathrm{e}}-\mathbf{q}} - \hbar\Omega - \mathrm{i}\eta_{\mathrm{h}}} + O(f^2). \qquad (13)$$

Here, we have also neglected all nonlinear carrier distribution contributions because we analyze the PSB luminescence only for dilute densities with $f \ll 1$. For quasistationary situations, Eqs. (12) and (13) are a static source initiating Υ^{em} correlations. At this level, Eq. (10) contains only one additional unknown triplet source, $\Delta\langle D^{\dagger}a^{\dagger}_{\mathrm{v}}a^{\dagger}_{\mathrm{c}}a_{\mathrm{c}}a_{\mathrm{c}}\rangle$. This is also a steady-state source that can conveniently be treated after we introduce the exciton basis discussed in Appendix A. After these formal steps, we eventually obtain

$$\begin{aligned}
&\sum_{\mathbf{k}'}\Delta\left\langle D^{\dagger}_{\mathbf{p}_{3\mathrm{D}}} a^{\dagger}_{\mathrm{c},\,\mathbf{k}'-\mathbf{p}_{\mathrm{h}}} a^{\dagger}_{\mathrm{v},\,\mathbf{k}-\mathbf{Q}_{\mathrm{h}}} a_{\mathrm{c},\,\mathbf{k}+\mathbf{Q}_{\mathrm{e}}} a_{\mathrm{v},\,\mathbf{k}'-\mathbf{p}_{\mathrm{h}}-\mathbf{q}}\right\rangle \\
&= \left[\phi^{\mathrm{R}}_{1s,\,\mathbf{q}}(\mathbf{0})\right]^{\star}\phi^{\mathrm{R}}_{1s,\,\mathbf{q}+\mathbf{p}}(\mathbf{k})\frac{\hbar\Omega\,\Delta N_{1s,\mathbf{q}+\mathbf{p}}}{E_{1s,\mathbf{q}+\mathbf{p}} - E_{1s,\mathbf{q}} - \hbar\Omega - \mathrm{i}\eta_{\mathrm{X}}}\cdot\sum_{\mathbf{k}'}\phi^{\mathrm{L}}_{1s,\,\mathbf{q}}(\mathbf{k}'-\mathbf{p}_{\mathrm{h}})\left[g^{\mathrm{c}}_{\mathbf{p}_{3\mathrm{D}}}\phi^{\mathrm{R}}_{1s,\,\mathbf{q}+\mathbf{p}}(\mathbf{k}') - g^{\mathrm{v}}_{\mathbf{p}_{3\mathrm{D}}}\phi^{\mathrm{R}}_{1s,\,\mathbf{q}+\mathbf{p}}(\mathbf{k}'-\mathbf{p})\right]^{\star}, \qquad (14)
\end{aligned}$$

where $\phi^{\mathrm{L}}_{\nu,\mathbf{q}}(\mathbf{k})$ and $\phi^{\mathrm{R}}_{\nu,\mathbf{q}}(\mathbf{k})$ refer to left- and right-handed excitonic wave functions, respectively, with the eigenenergy $E_{\lambda,\mathbf{q}}$. The exciton wave function in $\mathbf{r}$-space origin is defined by

$$\phi^{\mathrm{R}}_{\nu,\mathbf{q}}(\mathbf{0}) \equiv \sum_{\mathbf{k}} \phi^{\mathrm{R}}_{\nu,\mathbf{q}}(\mathbf{k}). \tag{15}$$

Equation (14) also contains the exciton distribution $\Delta N_{1s,\mathbf{q}}$ that follows strictly from the exciton correlation c_{X}. To study quasiequilibrium conditions, we assume that $\Delta N_{1s,\mathbf{q}}$ follows a Bose–Einstein distribution. In reality, $\Delta N_{1s,\mathbf{q}}$ can have a significant hole burning[29] close to $\mathbf{q} = \mathbf{0}$. However, this does not effect Eq. (14) much because $\Delta N_{1s,\mathbf{q}}$ appears within an integral. The solutions of Eq. (10) enter the photon-assisted polarization from Eq. (4) as an additional source weighted by the phonon-matrix elements $g^{\mathrm{c}}_{\mathbf{p}_{3\mathrm{D}}}$ and $g^{\mathrm{v}}_{\mathbf{p}_{3\mathrm{D}}}$, which can either be calculated via Fröhlich coupling[37–40] or deformation potential,[40–42] or a mixture of both.[36]

In our numerical studies, the complete set of equations is evaluated fully dynamically by solving the equations of motion as shown above. Generally, $\Upsilon^{\mathrm{em}}_{\mathbf{k},\mathbf{q}_{3\mathrm{D}},\mathbf{p}_{3\mathrm{D}}}$ has a full vectorial dependence on all $\mathbf{k}$, $\mathbf{q}_{3\mathrm{D}}$, and $\mathbf{p}_{3\mathrm{D}}$ coordinates, i.e., Υ^{em} contains, in principle, also a dependence of angles between $\mathbf{k}$, $\mathbf{q}_{3\mathrm{D}}$, and $\mathbf{p}_{3\mathrm{D}}$. However, the photon momentum $\mathbf{q}_{3\mathrm{D}}$ is extremely small in the typical scale of carrier and phonon momenta. In addition, the introduction of center-of-mass decomposition shown in Eq. (5) separates the $\mathbf{k}$ and $\mathbf{p}_{3\mathrm{D}}$ dependencies into angle-independent $\epsilon^{\mu}_{\mathbf{k}}$ and $\epsilon^{M}_{\mathbf{Q}} \simeq \epsilon^{M}_{\mathbf{p}}$ parts. Therefore, the angle dependence of $\Upsilon^{\mathrm{em}}_{\mathbf{k},\mathbf{q}_{3\mathrm{D}},\mathbf{p}_{3\mathrm{D}}}$ stems directly from $f^{\lambda}_{\mathbf{k}\pm\mathbf{q}_{\lambda}}$ parts emerging in the driving source. For typical $\mathbf{k}$ and $\mathbf{Q} \simeq \mathbf{p}$ ranges of phonon-assisted processes, this angle dependence is very weak. Therefore, we can substitute $\Upsilon^{\mathrm{em}}_{\mathbf{k},\mathbf{q}_{3\mathrm{D}},\mathbf{p}_{3\mathrm{D}}} \rightarrow \Upsilon^{\mathrm{em}}_{|\mathbf{k}|,|\mathbf{q}_{3\mathrm{D}}|,|\mathbf{p}_{3\mathrm{D}}|}$ to accurately describe the main effects of phonon-assisted emission. In the computations, we discretize Υ^{em} to $40 \times 40 \times 100 = 1.6 \times 10^5$ elements, which makes the dynamical calculation very intricate and time consuming already for the first phonon sideband.

For the computation, we have used typical ZnO parameters. The effective polaron mass of the electrons in ZnO can be determined very precisely in cyclotron-resonance measurement giving $m^{\mathrm{e}}_{\mathrm{eff}} = 0.28 m_0$.[5,43] The effective mass of the holes is $m^{\mathrm{h}}_{\mathrm{eff}} = 0.59 m_0$,[5] which produces a reduced mass of $\mu = 0.19 m_0$. The material parameters of the ZnO-type QW are chosen to produce a band gap of $E_{\mathrm{gap}} = 3.37$ eV[3,5,44] and an exciton binding energy of $E_{\mathrm{B}} = 60$ meV. The energy of the longitudinal-optical phonons is $\hbar\Omega = 72$ meV and we use the deformation potential with a coupling constant of $d_0^{\mathrm{opt.\,def.}} = 50.6$ eV. The refractive index of ZnO is listed with values between 2.0 and 2.2 in the literature.[45–47] In this work, the refractive index of the QW is assumed to be $n = 2.2$.

IV. PRINCIPAL EFFECTS OF THE CAVITY

Even though ZnO microcavities have not yet been realized experimentally, sample growth techniques are developing in a direction where one can grow ZnO-type QWs between distributed Bragg reflector (DBR) mirror pairs constructed from alternating ZnO/$Mg_{0.36}Zn_{0.64}O$ layers. The refractive index profile in this study consists of several planar sections

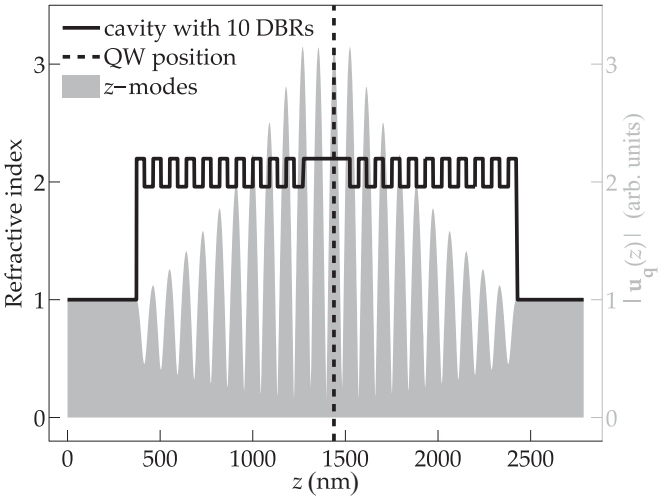

FIG. 1. Semiconductor microcavity structure. The refractive index profile of 10 ZnO/$Mg_{0.36}Zn_{0.64}O$ mirrors (black solid line) is shown together with an example of a resonant light mode $|\mathbf{u}_{\mathbf{q}}(z)|$ (shaded area). The quantum well is positioned at the mode maximum (dashed line) and the cavity has an optical thickness of $3/2\lambda$.

with piecewise constant $n = n(z)$. Each ZnO layer has the refractive index $n_{\mathrm{ZnO}} = 2.2$, while the $Mg_{0.36}Zn_{0.64}O$ layers have $n_{\mathrm{MgZnO}} = 1.96$.[46–49] For the cavity layer, we assume a material which shows the same refractive index as the ZnO-type QW itself to avoid reflections inside the sample structure. Figure 1 presents an exemplary microcavity $n(z)$ (solid line) and the mode function $u_{\mathbf{q}}(z)$ (shaded area) for the cavity resonance. The QW is positioned at the maximum of the mode function (dashed line).

The energetic position of the cavity resonance can be moved by adjusting the thickness of the $\lambda/4$ layers of the DBRs and the $3/2\lambda$ cavity layer, where λ is the wavelength of the cavity mode. Therefore, we can detune the cavity mode to be resonant either with the exciton resonance or the first PSB located at $E_{1s} - \hbar\Omega$. In the following, "1s cavity" refers to the case where the cavity is resonant with the 1s-exciton peak, i.e., the ZPL. The "phonon cavity" refers to a situation where the cavity is resonant with the PSB_1.

It is well known that the 1s cavity should produce a NMC splitting of the exciton peak into two peaks if the stimulated coupling between the light and the QW is strong enough.[24–26] Figure 2(a) shows the computed PL spectrum (black solid line) resulting from the 1s cavity. We have also plotted the bare cavity reflection (dark area) and the QW PL without the cavity (light-shaded area). The cavity mode and the 1s peak are clearly resonant, as they should be for the 1s-cavity configuration. The cavity in this example has 34 DBR layers producing a high 99.9% reflectivity for the mirrors.

As we compare the PL with (solid line) and without (light-shaded area) the cavity, we observe major qualitative changes. The 1s splits into two, as it should for the high-quality cavity, yielding the typical NMC scenario. At the same time, the overall level of the cavity PL is lower than without the cavity. Since NMC is the predominant process in this case, the phonon peak is very low. Other than that, the cavity does not modify the PSB_1 and the spectral shape of the emission at higher excitonic states. These aspects are studied further in Fig. 4.

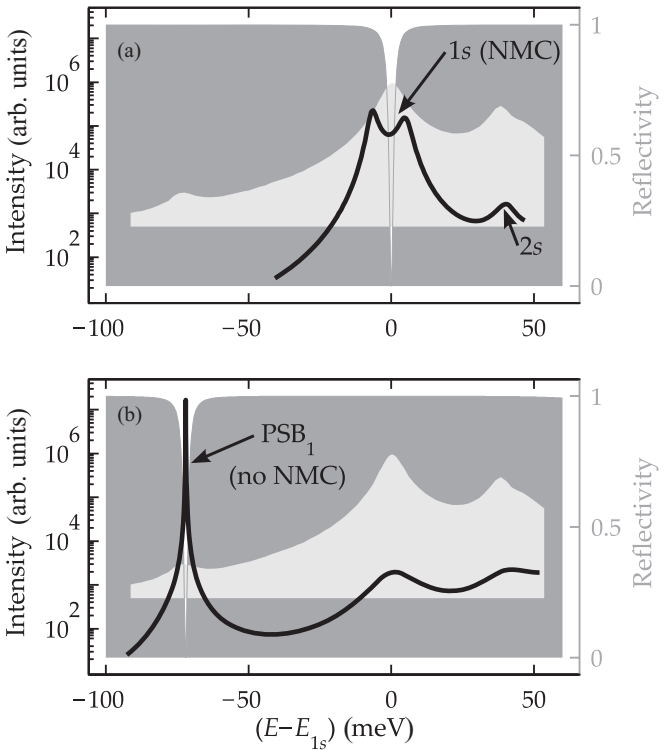

FIG. 2. Microcavity luminescence including the zero-phonon line (ZPL) and the first phonon sideband (PSB_1). The cavity is resonant with (a) the ZPL or (b) the PSB_1. The luminescence spectra with (solid line) and without (light area) cavity are compared with the reflectivity (dark area) of the bare cavity.

A completely different situation is observed in the phonon cavity where the cavity mode coincides with the first phonon sideband. In Fig. 2(b), we plot the resulting PL spectrum (solid line) showing that the phonon resonance is highly enhanced by the cavity, whereas the exciton resonance is suppressed. At the same time, the cavity PSB_1 does not produce a splitting of the emission resonance, indicating a fundamental difference between the 1*s*-cavity and the phonon–cavity coupling. For the 1*s* cavity, NMC follows from the reversible emission and absorption of light at the excitonic energy. For the phonon cavity, however, the cavity-PSB_1 coupling consists only of the photon emission part since one has only negligible phonon populations at low temperatures. Hence, there cannot be a reversible emission-absorption cycle and thus no NMC for the PSB.

A. Cavity effects vs mirror reflectivity

To verify that the phonon cavity does not produce NMC, we scan the PL spectra as a function of the DBR mirror pairs. This essentially increases the mirror reflectivity such that cavity effects become enhanced, producing a stronger coupling of the light modes to the material. Figure 3 shows the position of the emission peak(s) as a function of the DBR mirror pairs. One can clearly see that the 1*s* cavity produces a bifurcation of the 1*s* resonance into NMC splitting (solid line) as the mirror number is increased. At this point, the

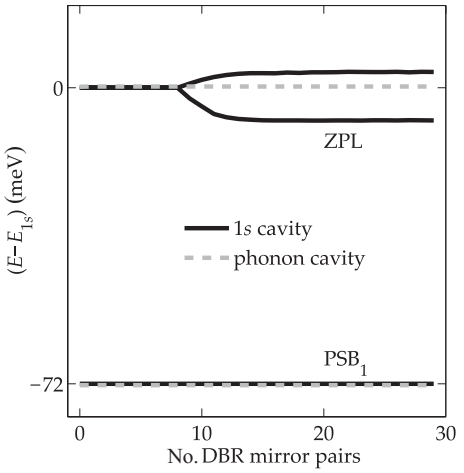

FIG. 3. Peak position in dependence of the number of DBR mirror pairs. The solid lines (dashed lines) indicate energies of the PL peaks for the 1*s* (phonon) cavity, respectively.

stimulated emission overcomes the spontaneous processes and the 1*s* resonance splits up into two peaks. The PSB_1 position, however, remains unchanged, indicating that the 1*s* cavity does not yield reversibility in this case. The phonon cavity produces a qualitatively very different behavior, as shown by the dashed lines. Neither the ZPL nor the PSB_1 positions are changed regardless of how strong the cavity becomes. This verifies that the PSB cannot yield to a reversible photon emission–absorption cycle due to a lack of phonon-assisted absorption, as discussed above.

The reversibility of the emission strongly alters the PL intensity, as seen in Fig. 2. To investigate this phenomenon further, in Fig. 4, we show the integrated PL around the 1*s*

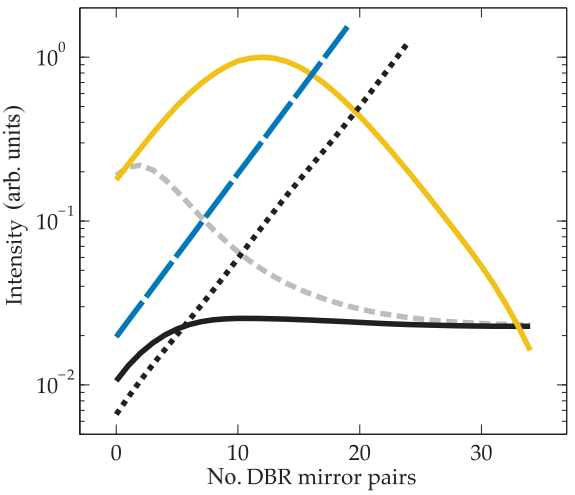

FIG. 4. (Color online) Intensity of the photoluminescence spectrum. The yellow (light gray) solid line shows the intensity of the exciton resonance for the 1*s* cavity, whereas the intensity of the phonon peak in the phonon cavity is shown by the black solid line. The short-dashed line shows the total intensity in the phonon cavity. The mode function maximum and the peak height of the first phonon sideband are indicated by the long-dashed (blue) and the dotted (black) lines, respectively.

(yellow solid line) and the PSB_1 (black solid line) resonances for the phonon cavity as a function of DBR mirror pairs. We also have defined the PSB_1 peak height (dotted line) and total integrated PL (dashed line) together with the mode strength $|u_{\mathbf{q}}|^2$ at the position of the QW.

In case of the $1s$ cavity, the intensity of ZPL emission (yellow solid line) first increases rapidly. However, the onset of reversibility starts to decrease the ZPL intensity assigning the regime of NMC. This transition takes place around 8 DBRs, which is the same threshold value producing NMC splitting in Fig. 3.

The phonon cavity produces a very different behavior. The integrated PSB_1 intensity (black solid line) first starts to increase slightly and then saturates to a constant level. In particular, we do not observe any decrease in the integrated PSB_1 intensity. At the same time, the PSB_1 peak height (dotted line) increases monotonously with the cavity mode strength (long-dashed blue line). These two observations mean that the cavity first enhances the PSB_1 via the Purcell effect. For an elevated number of DBR pairs, the PSB_1 narrows since the peak emission grows while the total emission saturates. Interestingly, the strong-cavity limit exclusively favors the PSB_1 emission over the ZPL emission because the integrated total PL (gray dashed line) and PSB_1 emission (black solid line) become equal.

V. ANALYTIC MODEL

To better understand the physical origin of the found effects, we develop an analytic model that captures the essence of the microcavity luminescence of the ZPL and PSB_1 emission. Here, we include only the $1s$ contributions and limit the investigation to dilute densities with $f^{\mathrm{e}} \ll 1$ and $f^{\mathrm{h}} \ll 1$. In this situation, it is beneficial to convert the full Eqs. (2), (4), (10), and (11) into the exciton basis,

$$\Pi^{X}_{\nu,\mathbf{q}_{3\mathrm{D}}} = \sum_{\mathbf{k}} \phi^{\star}_{\nu}(\mathbf{k})\, \Pi_{\mathbf{k},\mathbf{q}_{3\mathrm{D}}}, \tag{16a}$$

$$\Pi_{\mathbf{k},\mathbf{q}_{3\mathrm{D}}} = \sum_{\nu} \phi_{\nu}(\mathbf{k})\, \Pi^{X}_{\nu,\mathbf{q}_{3\mathrm{D}}}, \tag{16b}$$

and

$$\Upsilon^{X}_{\nu,\mathbf{p}_{3\mathrm{D}},\mathbf{q}_{3\mathrm{D}}} = \sum_{\mathbf{k}} \phi^{\star}_{\nu}(\mathbf{k})\, \Upsilon_{\mathbf{k},\mathbf{q}_{3\mathrm{D}},\mathbf{p}_{3\mathrm{D}}}, \tag{17a}$$

$$\Upsilon_{\mathbf{k},\mathbf{q}_{3\mathrm{D}},\mathbf{p}_{3\mathrm{D}}} = \sum_{\nu} \phi_{\nu}(\mathbf{k})\, \Upsilon^{X}_{\nu,\mathbf{p}_{3\mathrm{D}},\mathbf{q}_{3\mathrm{D}}}. \tag{17b}$$

For nonvanishing densities, one must distinguish the excitonic wave functions into left- and right-handed, i.e., $\phi^{\mathrm{L}}_{\nu,\mathbf{Q}}(\mathbf{k})$ and $\phi^{\mathrm{R}}_{\nu,\mathbf{Q}}(\mathbf{k})$. See the discussion in Appendix A for further details. Projecting the $1s$ component of Eq. (4) converts the principal structure of the SLE into

$$\mathrm{i}\hbar\frac{\partial}{\partial t}\Pi^{X}_{1s,\mathbf{q}_{3\mathrm{D}}} = [E_{1s,\mathbf{q}} - \hbar\omega_{\mathbf{q}_{3\mathrm{D}}} - \mathrm{i}\gamma_0]\Pi^{X}_{1s,\mathbf{q}_{3\mathrm{D}}} - \mathrm{i}\sum_{q'_{\perp}} \mathcal{F}^{1s}_{\mathbf{q},q'_{\perp}}\, \Delta\langle B^{\dagger}_{\mathbf{q}_{3\mathrm{D}}} B_{\mathbf{q},q'_{\perp}}\rangle + \mathrm{i}\mathcal{F}^{1s}_{\mathbf{q}_{3\mathrm{D}}} N_{1s,\mathbf{q}} + \hbar\Omega \sum_{\mathbf{p}_{3\mathrm{D}}} g^{1s,1s}_{\mathbf{p}_{3\mathrm{D}}}\, \Upsilon^{X}_{1s,\mathbf{p},\mathbf{q}_{3\mathrm{D}}}, \tag{18}$$

$$\mathrm{i}\hbar\frac{\partial}{\partial t}\Delta\langle B^{\dagger}_{\mathbf{q}_{3\mathrm{D}}} B_{\mathbf{q},q'_{\perp}}\rangle = (\hbar\omega_{\mathbf{q},q'_{\perp}} - \hbar\omega_{\mathbf{q}_{3\mathrm{D}}})\Delta\langle B^{\dagger}_{\mathbf{q}_{3\mathrm{D}}} B_{\mathbf{q},q'_{\perp}}\rangle + \mathrm{i}[\mathcal{F}^{1s}_{\mathbf{q},q'_{\perp}}]^{\star}\Pi^{X}_{1s,\mathbf{q}_{3\mathrm{D}}} + \mathrm{i}\mathcal{F}^{1s}_{\mathbf{q}_{3\mathrm{D}}}[\Pi^{X}_{1s,\mathbf{q},q'_{\perp}}]^{\star}, \tag{19}$$

where the source term $N_{1s} = N^{\mathrm{eh}}_{1s} + \Delta N_{1s}$ is decomposed into a singlet and a correlated contribution. For low densities, the singlet part is proportional to $f^{\mathrm{e}} f^{\mathrm{h}}$ such that the spontaneous emission source follows mostly from the exciton distribution $N_{1s,\mathbf{q}} = \Delta N_{1s,\mathbf{q}}$ if it exists.[50] The quantity $\mathcal{F}^{1s}_{\mathbf{q}_{3\mathrm{D}}} \equiv \phi_{1s}(\mathbf{0})\, \mathcal{F}_{\mathbf{q}_{3\mathrm{D}}}$ defines the strength of the spontaneous emission.

Following the same derivation steps as in Eq. (18), the triplet source becomes

$$\mathrm{i}\hbar\frac{\partial}{\partial t}\Upsilon^{X}_{1s,\mathbf{p},\mathbf{q}_{3\mathrm{D}}} = \big[E_{1s,\mathbf{q}+\mathbf{p}} - \hbar\omega_{\mathbf{q}_{3\mathrm{D}}} - \hbar\Omega - \mathrm{i}\gamma_1\big]\Upsilon^{X}_{1s,\mathbf{p},\mathbf{q}_{3\mathrm{D}}} - \mathrm{i}\sum_{q'_{\perp}} \mathcal{F}^{1s}_{\mathbf{q}+\mathbf{p},q'_{\perp}}\, \Delta\langle D^{\dagger}_{\mathbf{p}_{3\mathrm{D}}} B^{\dagger}_{\mathbf{q}_{3\mathrm{D}}} B_{\mathbf{q}+\mathbf{p},q'_{\perp}}\rangle + \mathrm{i}\mathcal{F}^{1s}_{\mathbf{q}_{3\mathrm{D}}}\Delta N_{1s,\mathbf{p}_{3\mathrm{D}}}, \tag{20}$$

$$\begin{aligned}\mathrm{i}\hbar\frac{\partial}{\partial t}\Delta\langle D^{\dagger}_{\mathbf{p}_{3\mathrm{D}}} B^{\dagger}_{\mathbf{q}_{3\mathrm{D}}} B_{\mathbf{q}+\mathbf{p},q'_{\perp}}\rangle &= (\hbar\omega_{\mathbf{q}+\mathbf{p},q'_{\perp}} - \hbar\omega_{\mathbf{q}_{3\mathrm{D}}} - \hbar\Omega)\Delta\langle D^{\dagger}_{\mathbf{p}_{3\mathrm{D}}} B^{\dagger}_{\mathbf{q}_{3\mathrm{D}}} B_{\mathbf{q}+\mathbf{p},q'_{\perp}}\rangle \\ &\quad + \mathrm{i}\mathcal{F}^{1s}_{\mathbf{q}_{3\mathrm{D}}}\Delta\langle D^{\dagger}_{\mathbf{p}_{3\mathrm{D}}} B^{\dagger}_{\mathbf{q}+\mathbf{p},q'_{\perp}} X_{1s,\mathbf{q}}\rangle^{\star} + \mathrm{i}[\mathcal{F}^{1s}_{\mathbf{q}+\mathbf{p},q'_{\perp}}]^{\star}\Upsilon^{X}_{1s,\mathbf{p},\mathbf{q}_{3\mathrm{D}}}.\end{aligned} \tag{21}$$

The Υ^{X} dynamics contains a spontaneous phonon-assisted source,

$$\Delta N_{1s,\mathbf{p}_{3\mathrm{D}}} = \frac{\hbar\Omega\,[g^{1s,1s}_{\mathbf{p}_{3\mathrm{D}}}]^{\star}\Delta N_{1s,\mathbf{p}}}{E_{1s,\mathbf{p}} - E_{1s,\mathbf{0}} - \hbar\Omega} = \frac{\hbar\Omega\,[g^{1s,1s}_{\mathbf{p}_{3\mathrm{D}}}]^{\star}\Delta N_{1s,\mathbf{p}}}{\epsilon^{M}_{\mathbf{p}} - \hbar\Omega}, \tag{22}$$

where we have introduced the strength by the excitonic phonon-matrix element

$$g^{1s,1s}_{\mathbf{p}_{3\mathrm{D}}} = \sum_{\mathbf{k}'} \phi_{1s}(\mathbf{k}')\big[g^{\mathrm{c}}_{\mathbf{p}_{3\mathrm{D}}}\phi_{1s}(\mathbf{k}' + \mathbf{p}_{\mathrm{h}}) - g^{\mathrm{v}}_{\mathbf{p}_{3\mathrm{D}}}\phi_{1s}(\mathbf{k}' - \mathbf{p}_{\mathrm{e}})\big]^{\star}. \tag{23}$$

These contributions describe phonon-assisted processes between two exciton states.

A. Treatment of the stimulated parts

Even though the limitation to the $1s$-exciton contributions reduces the complexity of the phonon-assisted SLE considerably, Eqs. (18) and (20) still contain the nontrivial stimulated coupling via the $\sum \mathcal{F}\Delta\langle B^\dagger B\rangle$ and $\sum \mathcal{F}\Delta\langle D^\dagger B^\dagger B\rangle$ dependent contributions. To deal with these parts analytically, we introduce a scaled photon-operator and photon-assisted polarization

$$\bar{B}_{\mathbf{q},q_\perp'} \equiv \frac{B_{\mathbf{q},q_\perp'}}{\left[\mathcal{F}^{1s}_{\mathbf{q},q_\perp'}\right]^\star}, \tag{24}$$

$$\bar{\Pi}^X_{1s,\mathbf{q}_{3D}} \equiv \frac{\Pi^X_{1s,\mathbf{q}_{3D}}}{\mathcal{F}^{1s}_{\mathbf{q}_{3D}}}, \tag{25}$$

respectively. To solve Eqs. (18) and (19), we furthermore introduce collective operators

$$\bar{B}^\dagger_{\mathbf{q},\Sigma} \equiv \frac{1}{\mathcal{G}}\sum_{q_\perp'}\left[\mathcal{F}^{1s}_{\mathbf{q},q_\perp'}\right]^\star B^\dagger_{\mathbf{q},q_\perp'} = \frac{1}{\mathcal{G}}\sum_{q_\perp'}\left|\mathcal{F}^{1s}_{\mathbf{q},q_\perp'}\right|^2 \bar{B}^\dagger_{\mathbf{q},q_\perp'}, \tag{26a}$$

$$\bar{B}_{\mathbf{q},\Sigma} \equiv \frac{1}{\mathcal{G}}\sum_{q_\perp'}\mathcal{F}^{1s}_{\mathbf{q},q_\perp'} B_{\mathbf{q},q_\perp'} = \frac{1}{\mathcal{G}}\sum_{q_\perp'}\left|\mathcal{F}^{1s}_{\mathbf{q},q_\perp'}\right|^2 \bar{B}_{\mathbf{q},q_\perp'}. \tag{26b}$$

It is convenient to choose a normalization $\mathcal{G}$ such that $\bar{B}^\dagger_{\mathbf{q},\Sigma}$ and $\bar{B}_{\mathbf{q},\Sigma}$ satisfy Bosonic commutation relations. More specifically, we find Bosonic commutation $[\bar{B}_{\mathbf{q},\Sigma},\bar{B}^\dagger_{\mathbf{q}',\Sigma}]_- = 1$ if $\mathcal{G}^2 = \sum_{q_\perp}|\mathcal{F}^{1s}_{\mathbf{q},q_\perp}|^2$. To see the usefulness of the effective mode (26a) and (26b), we start by computing its dynamics from Eq. (19):

$$\begin{aligned}\mathrm{i}\hbar\frac{\partial}{\partial t}\Delta\langle\bar{B}^\dagger_{\mathbf{q},\Sigma}\bar{B}_{\mathbf{q},\Sigma}\rangle = {}& \frac{1}{\mathcal{G}^2}\sum_{q_\perp,q_\perp'}\left[\mathcal{F}^{1s}_{\mathbf{q},q_\perp}\right]^\star\mathcal{F}^{1s}_{\mathbf{q},q_\perp'}(\hbar\omega_{\mathbf{q},q_\perp'}-\hbar\omega_{\mathrm{cav}})\Delta\langle B^\dagger_{\mathbf{q},q_\perp}B_{\mathbf{q},q_\perp'}\rangle \\ & + \frac{1}{\mathcal{G}^2}\sum_{q_\perp,q_\perp'}\left[\mathcal{F}^{1s}_{\mathbf{q},q_\perp}\right]^\star\mathcal{F}^{1s}_{\mathbf{q},q_\perp'}(\hbar\omega_{\mathrm{cav}}-\hbar\omega_{\mathbf{q},q_\perp})\Delta\langle B^\dagger_{\mathbf{q},q_\perp}B_{\mathbf{q},q_\perp'}\rangle + 2\mathrm{i}\mathcal{G}\,\mathrm{Re}\left[\bar{\Pi}^X_{1s,\mathbf{q},\Sigma}\right],\end{aligned} \tag{27}$$

where we identified a collective photon-assisted contribution

$$\bar{\Pi}^X_{1s,\mathbf{q},\Sigma} \equiv \frac{1}{\mathcal{G}}\sum_{q_\perp'}\left|\mathcal{F}^{1s}_{\mathbf{q},q_\perp'}\right|^2\bar{\Pi}^X_{1s,\mathbf{q},q_\perp'}, \tag{28}$$

in analogy to Eq. (26a).

To study the case where the stimulated effects are particularly strong, we consider the situation of a planar semiconductor microcavity, as shown by the solid black line in Fig. 1. The cavity mode $|u_{\mathbf{q}}(z)|$ shown by the gray-shaded area is concentrated inside the cavity and the QW is positioned at one of the mode maxima, z_{QW}. The corresponding mode strength $|\mathcal{F}^{1s}_{\mathbf{q},q_\perp}|^2 \propto |u_{\mathbf{q},q_{\mathrm{cav}}}(z_{\mathrm{QW}})|^2$ forms a narrow peak around the cavity-mode energy $E_{\mathrm{cav}} = \hbar\omega_{\mathrm{cav}}$, whereas the area under $|\mathcal{F}^{1s}_{\mathbf{q},q_\perp}|^2$ remains unchanged when increasing the number of DBR layers, i.e., narrowing the peak width. Eventually, the cavity mode approaches a δ function as the cavity becomes stronger. Therefore, we can apply the *strong-cavity approximation* (SCA)

$$\sum_{q_\perp}\left|\mathcal{F}^{1s}_{\mathbf{q},q_\perp}\right|^2(\omega_{\mathbf{q},q_\perp}-\omega_{\mathrm{cav}})\odot_{\mathbf{q},q_\perp} = 0 \tag{29}$$

whenever $|\mathcal{F}^{1s}_{\mathbf{q},q_\perp}|^2$ is strongly peaked around ω_{cav} and the function $\odot_{\mathbf{q},q_\perp}$ is a slowly varying function around $\omega_{\mathbf{q},q_\perp} = \omega_{\mathrm{cav}}$. The SCA converts Eqs. (18) and (27) into

$$\mathrm{i}\hbar\frac{\partial}{\partial t}\Delta\langle\bar{B}^\dagger_{\mathbf{q},\Sigma}\bar{B}_{\mathbf{q},\Sigma}\rangle = 2\mathrm{i}\mathcal{G}\,\mathrm{Re}\left[\bar{\Pi}^X_{1s,\mathbf{q},\Sigma}\right], \tag{30}$$

$$\begin{aligned}\mathrm{i}\hbar\frac{\partial}{\partial t}\bar{\Pi}^X_{1s,\mathbf{q},\Sigma} = {}& [E_{1s,\mathbf{0}}-\hbar\omega_{\mathrm{cav}}-\mathrm{i}\gamma_0]\bar{\Pi}^X_{1s,\mathbf{q},\Sigma} \\ & + \mathrm{i}\,\mathcal{G}(\Delta N_{1s,\mathbf{0}} - \Delta\langle\bar{B}^\dagger_{\mathbf{0},\Sigma}\bar{B}_{\mathbf{0},\Sigma}\rangle) \\ & + \sum_{\mathbf{p}}\Delta\langle\bar{D}^\dagger_{\mathbf{p},\Sigma}\bar{B}^\dagger_{\mathbf{0},\Sigma}X_{\mathbf{p}}\rangle,\end{aligned} \tag{31}$$

where we defined a collective phonon operator

$$\bar{D}_{\mathbf{p},\Sigma} \equiv \sum_{p_\perp}\bar{D}_{\mathbf{p},p_\perp} \tag{32}$$

with

$$\bar{D}_{\mathbf{p},p_\perp} = \bar{D}_{\mathbf{p}_{3D}} \equiv \hbar\Omega\, g^{\nu,\nu'}_{\mathbf{p}_{3D}} D_{\mathbf{p}_{3D}}. \tag{33}$$

In the following, we study normal emission such that we can set $\mathbf{q} = \mathbf{0}$ in the photon operators. To keep the expressions brief, we introduce

$$\Delta^{\mathrm{ZPL}}_{\omega,\mathbf{p}} \equiv E_{1s,\mathbf{p}} - \hbar\omega_{\mathbf{0},q_\perp}, \tag{34a}$$

$$\Delta^{\mathrm{PSB},\pm}_{\omega,\mathbf{p}} \equiv E_{1s,\mathbf{p}} - \hbar\omega_{\mathbf{0},q_\perp} \pm \hbar\Omega, \tag{34b}$$

$$\Delta^{\mathrm{cav}}_{\omega} \equiv \hbar\omega_{\mathrm{cav}} - \hbar\omega_{\mathbf{0},q_\perp}, \tag{34c}$$

which define the exciton–light detuning ($\Delta^{\mathrm{ZPL}}_{\omega,\mathbf{p}}$), the PSB–light detuning ($\Delta^{\mathrm{PSB},\pm}_{\omega,\mathbf{p}}$), and the cavity–light detuning ($\Delta^{\mathrm{cav}}_{\omega}$), respectively. To solve the PL in the normal direction, we insert the transformations (26a), (26b), and (28) into Eqs. (18) and

(19). With similar steps as those producing Eqs. (30) and (31), we now obtain

$$\mathrm{i}\hbar\frac{\partial}{\partial t}\begin{pmatrix}\bar{\Pi}^{X}_{1s,\mathbf{0},q_\perp}\\ \Delta\langle\bar{B}^{\dagger}_{\mathbf{0},q_\perp}\bar{B}_{\mathbf{0},\Sigma}\rangle\end{pmatrix} = \mathbf{M}\begin{pmatrix}\bar{\Pi}^{X}_{1s,\mathbf{0},q_\perp}\\ \Delta\langle\bar{B}^{\dagger}_{\mathbf{0},q_\perp}\bar{B}_{\mathbf{0},\Sigma}\rangle\end{pmatrix} + \begin{pmatrix}\mathrm{i}\,\Delta N_{1s,\mathbf{0}} + \sum_{\mathbf{p}}\Delta\langle\bar{D}^{\dagger}_{\mathbf{p},\Sigma}\bar{B}^{\dagger}_{\mathbf{0},q_\perp}X_{\mathbf{p}}\rangle\\ \mathrm{i}\left[\bar{\Pi}^{X}_{1s,\mathbf{0},\Sigma}\right]^{\star}\end{pmatrix}, \tag{35}$$

where we have identified a 2×2 matrix,

$$\mathbf{M} = \begin{pmatrix}\Delta^{\mathrm{ZPL}}_{\omega,\mathbf{0}} - \mathrm{i}\gamma_0 & -\mathrm{i}\,\mathcal{G}\\ \mathrm{i}\,\mathcal{G} & \Delta^{\mathrm{cav}}_{\omega}\end{pmatrix}. \tag{36}$$

The dynamics of Eq. (35) follows from a closed set of equations only in the absence of phonon effects.

Before we analyze the full PSB emission, we develop a suitable solution algorithm by solving Eqs. (30), (31), and (35) without phonons. We start from the steady state of Eq. (31), producing

$$\bar{\Pi}^{X}_{1s,\mathbf{0},\Sigma} = \mathrm{i}\,\mathcal{G}\frac{\Delta\langle\bar{B}^{\dagger}_{\mathbf{0},\Sigma}\bar{B}_{\mathbf{0},\Sigma}\rangle - \Delta N_{1s,\mathbf{0}}}{E_{1s,\mathbf{0}} - \hbar\omega_{\mathrm{cav}} - \mathrm{i}\gamma_0}. \tag{37}$$

This result implies that $\Delta\langle\bar{B}^{\dagger}_{\mathbf{0},\Sigma}\bar{B}_{\mathbf{0},\Sigma}\rangle$ is driven and a steady state is not reached unless we demand $\mathrm{Re}[\bar{\Pi}^{X}_{1s,\mathbf{q},\Sigma}]\equiv 0$; compare with Eq. (30). This leads to the constant collective photon-number correlation,

$$\Delta\langle\bar{B}^{\dagger}_{\mathbf{0},\Sigma}\bar{B}_{\mathbf{0},\Sigma}\rangle = \Delta N_{1s,\mathbf{0}}, \tag{38}$$

in the steady state. For this choice, $\bar{\Pi}^{X}_{1s,\mathbf{0},\Sigma}$ vanishes such that Eq. (35) becomes

$$\mathrm{i}\hbar\frac{\partial}{\partial t}\begin{pmatrix}\bar{\Pi}^{X}_{1s,\mathbf{0},q_\perp}\\ \Delta\langle\bar{B}^{\dagger}_{\mathbf{0},q_\perp}\bar{B}_{\mathbf{0},\Sigma}\rangle\end{pmatrix} = \mathbf{M}\begin{pmatrix}\bar{\Pi}^{X}_{1s,\mathbf{0},q_\perp}\\ \Delta\langle\bar{B}^{\dagger}_{\mathbf{0},q_\perp}\bar{B}_{\mathbf{0},\Sigma}\rangle\end{pmatrix} + \begin{pmatrix}\mathrm{i}\,\Delta N_{1s,\mathbf{0}}\\ 0\end{pmatrix}. \tag{39}$$

This is now a typical linear equation driven by a known constant source $\Delta N_{1s,\mathbf{0}}$. Since $\mathbf{M}$ contains dephasing, Eq. (39) always evolves toward a steady state, yielding

$$\bar{\Pi}^{X}_{1s,\mathbf{0},q_\perp} = \frac{\mathrm{i}\,\Delta N_{1s,\mathbf{0}}\,(\hbar\omega_{\mathbf{0},q_\perp} - \hbar\omega_{\mathrm{cav}})}{\det[\mathbf{M}]}, \tag{40}$$

where $\det[\mathbf{M}] = (E_{1s,\mathbf{0}} - \hbar\omega_{\mathbf{0},q_\perp} - \mathrm{i}\gamma_0)\,(\hbar\omega_{\mathrm{cav}} - \hbar\omega_{\mathbf{0},q_\perp}) - \mathcal{G}^2$. To gain more insight, it is useful to rewrite the determinant via its roots:

$$\begin{aligned}\det[\mathbf{M}] &= \left(\Delta^{\mathrm{cav}}_{\omega} - \Delta_+\right)\left(\Delta^{\mathrm{cav}}_{\omega} - \Delta_-\right), \quad \text{with}\\ \Delta_\pm &= \tfrac{1}{2}\left(\Delta^{\mathrm{cav}}_{1s} + \mathrm{i}\gamma_0 \pm \Omega^{\mathrm{cav}}_{1s}\right),\\ \Omega^{\mathrm{cav}}_{1s} &= \sqrt{4\mathcal{G}^2 + \left(\Delta^{\mathrm{cav}}_{1s} + \mathrm{i}\gamma_0\right)^2}.\end{aligned} \tag{41}$$

By inserting Eqs. (41) into Eq. (40) and performing a partial-fraction decomposition, we can express $\bar{\Pi}^{X}_{1s,\mathbf{0},q_\perp}$ in terms of two individual Lorentzians,

$$\bar{\Pi}^{X}_{1s,\mathbf{0},q_\perp} = \frac{\mathrm{i}\,\Delta N_{1s,\mathbf{0}}}{\Delta_+ - \Delta_-}\left(\frac{\Delta_-}{\Delta^{\mathrm{cav}}_{\omega} - \Delta_-} - \frac{\Delta_+}{\Delta^{\mathrm{cav}}_{\omega} - \Delta_+}\right). \tag{42}$$

We can now evaluate the steady-state photon flux (3) that defines the photoluminescence spectrum,

$$I^{\mathrm{ZPL}}_{\mathrm{PL}}(\omega_{\mathbf{0},q_\perp}) = \frac{2}{\hbar}\left|\mathcal{F}^{1s}_{\mathbf{0},q_\perp}\right|^2\mathrm{Re}\left[\bar{\Pi}^{X}_{1s,\mathbf{0},q_\perp}\right] = \frac{2}{\hbar}\left|\mathcal{F}^{1s}_{\mathbf{0},q_\perp}\right|^2\mathrm{Re}\left[\frac{\mathrm{i}\,\Delta N_{1s,\mathbf{0}}}{\Delta_+ - \Delta_-}\left(\frac{\Delta_-}{\hbar\omega_{\mathrm{cav}} - \Delta_- - \hbar\omega_{\mathbf{0},q_\perp}} - \frac{\Delta_+}{\hbar\omega_{\mathrm{cav}} - \Delta_+ - \hbar\omega_{\mathbf{0},q_\perp}}\right)\right], \tag{43}$$

after the result (42) is used. We see now that the presence of a cavity splits the emission into two separate normal-mode coupling resonances centered at $\mathrm{Re}[\hbar\omega_{\mathrm{cav}} - \Delta_\pm]$. The corresponding width of the Lorentzians is defined by $\gamma_{0,\pm} = \mathrm{Im}[\Delta_\pm]$. Therefore, Eq. (43) provides an analytic model to study NMC PL.

The complete set including phonons is derived analogously by applying the new operator definitions and approximations several times to Eqs. (20) and (21), respectively. The results for the closed set of equations are presented in Appendix B. These equations will then evolve to a steady state.

B. Steady-state solution for the analytic model

The full analytic model, including PSB effects, is presented in Appendix B. We can apply the same derivation strategy as that which produces Eq. (43). Following this approach, the expression for the PL becomes

$$I_{\mathrm{PL}}(\omega_{\mathbf{0},q_\perp}) = \frac{2}{\hbar}\left|\mathcal{F}^{1s}_{\mathbf{0},q_\perp}\right|^2\mathrm{Re}\left[\bar{\Pi}^{X,\,\mathrm{ZPL}}_{1s,\mathbf{0},q_\perp} + \bar{\Pi}^{X,\,\mathrm{PSB}}_{1s,\mathbf{0},q_\perp}\right]. \tag{44}$$

The ZPL contribution $\bar{\Pi}^{X,\,\mathrm{ZPL}}_{1s,\mathbf{0},q_\perp}$ is defined by Eq. (42). The corresponding PSB contributions result from

$$\bar{\Pi}^{X,\,\mathrm{PSB}}_{1s,\mathbf{0},q_\perp} = \frac{\mathrm{i}[\mathcal{T}_1(\omega_{\mathbf{0},q_\perp}) - \mathcal{T}_2(\omega_{\mathbf{0},q_\perp})]\Delta^{\mathrm{cav}}_{\omega} - \frac{\mathrm{i}\,\mathrm{Im}[\mathcal{T}_3] + \mathcal{T}_1(\omega_{\mathrm{cav}})}{\gamma_0}\mathcal{G}^2}{\mathcal{G}^2 - \left(\Delta^{\mathrm{ZPL}}_{\omega,\mathbf{0}} - \mathrm{i}\gamma_0\right)\Delta^{\mathrm{cav}}_{\omega}}. \tag{45}$$

These contain the spectral function

$$\mathcal{T}_1(\omega_{\mathbf{0},q_\perp}) = \sum_{\mathbf{p}}\frac{\chi_{\mathbf{p}}}{\Delta^{\mathrm{PSB},-}_{\omega,\mathbf{p}} - \mathrm{i}\gamma_1}, \tag{46}$$

with the oscillator strength

$$\begin{aligned}\chi_{\mathbf{p}} &\equiv \sum_{p_\perp}\hbar\Omega\,g^{1s,1s}_{\mathbf{p}_{3\mathrm{D}}}\Delta N_{1s,\mathbf{p}_{3\mathrm{D}}} = \frac{\xi_{\mathbf{p}}}{\hbar\Omega - \frac{\hbar^2\mathbf{p}^2}{2M}},\\ \xi_{\mathbf{p}} &\equiv \Delta N_{1s,\mathbf{p}}\sum_{p_\perp}\left|\hbar\Omega\,g^{1s,1s}_{\mathbf{p}_{3\mathrm{D}}}\right|^2.\end{aligned} \tag{47}$$

The other spectral functions are

$$\mathcal{T}_2(\omega_{\mathbf{0},q_\perp}) = \frac{\chi_{\mathbf{0}}\left[\Delta_\omega^{\mathrm{cav}} - \hbar\Omega - \mathcal{GR}\right]}{\mathcal{G}^2 - \left[\Delta_\omega^{\mathrm{cav}} - \hbar\Omega\right]\left[\Delta_{\omega,\mathbf{0}}^{\mathrm{PSB},-} - \mathrm{i}\gamma_1\right]}, \quad (48)$$

$$\mathcal{T}_3 = \chi_{\mathbf{0}}\,\hbar\Omega\,\frac{\Delta_{\omega,\mathbf{0}}^{\mathrm{PSB},+} - \Delta_\omega^{\mathrm{cav}} - \mathrm{i}\gamma_1}{\mathcal{S}_-}, \quad (49)$$

containing quantities

$$\mathcal{R} = \mathcal{G}\hbar\Omega\frac{\Delta_{\omega,\mathbf{0}}^{\mathrm{PSB},-} - \Delta_\omega^{\mathrm{cav}} - \mathrm{i}\gamma_1}{\mathcal{S}_+}, \quad (50)$$

$$S_\pm = \left[\Delta_{\omega,\mathbf{0}}^{\mathrm{PSB},-}\Delta_{\omega,\mathbf{0}}^{\mathrm{PSB},+} + 2\mathcal{G}^2 + \gamma_1^2\right]\hbar\Omega \pm 2\mathrm{i}\gamma_1[\mathcal{G}^2 - \hbar^2\Omega^2], \quad (51)$$

where $S_\pm$ has an analogous structure to Eq. (41).

In the case of the PSB cavity, $\hbar\omega_{\mathrm{cav}}$ is equal to the PSB_1 energy $E_{1s,\mathbf{0}} - \hbar\Omega$. As a result, the detunings (34b) reduce into

$$\Delta_{\omega,\mathbf{0}}^{\mathrm{PSB},-} \to \Delta_\omega^{\mathrm{cav}} \quad \text{and} \quad \Delta_{\omega,\mathbf{0}}^{\mathrm{PSB},+} = 2\hbar\Omega + \Delta_\omega^{\mathrm{cav}} \to 2\hbar\Omega, \quad (52)$$

where the limit applies close to the cavity resonance. Since the phonon energy is relatively large, we may additionally apply $\hbar\Omega \gg \mathcal{G}$, $\hbar\Omega \gg \Delta_\omega^{\mathrm{cav}}$, and $\hbar\Omega \gg \gamma_{\{0,1\}}$. By implementing these limits to Eqs. (45) and (46), and (48)–(51), we find

$$\mathrm{Re}\left[\bar{\Pi}_{1s,\mathbf{0},q_\perp}^{X,\ \mathrm{PSB}}\right] \to \frac{\gamma_1\left[\chi_{\mathbf{0}} + \sum_{\mathbf{p}}\chi_{\mathbf{p}}\right]}{\left(\Delta_\omega^{\mathrm{cav}}\right)^2 + \gamma_1^2}. \quad (53)$$

These results show very clearly that the PSB does not produce a splitting of the PSB resonance. Instead, the cavity enhances the PSB luminescence, which can be applied to increase the visibility of the PSB emission.

C. PL intensity

The fully analytic luminescence formula (44) can directly be applied to deduce the integrated PL. In order to characterize the overall ZPL and PSB luminescence, we integrate the ZPL and the PSB_1 parts of Eq. (44) separately, i.e.,

$$\mathscr{I}_{\{1s,\,\mathrm{ph}\}}^{\{\mathrm{ZPL},\,\mathrm{PSB}\}}(\eta) = \int_{-\infty}^{\infty} I_{\mathrm{PL}}^{\{\mathrm{ZPL},\,\mathrm{PSB}\}}(\omega)\,\mathrm{d}\omega, \quad (54)$$

where $\hbar\omega_{\mathrm{cav}}$ was chosen to coincide with the $1s$ cavity (subindex "$1s$") or the phonon cavity (subindex "ph"). For the mode function, we assume a Lorentzian

$$|u(\omega)|^2 = \frac{\mathcal{E}_0}{\pi}\frac{\eta}{(\hbar\omega - \hbar\omega_{\mathrm{cav}})^2 + \eta^2}, \quad (55)$$

where $\mathcal{E}_0$ is an amplitude with the unit of an energy so that the mode function is unitless, $\hbar\omega_{\mathrm{cav}}$ is again the resonance energy of the cavity mode, and η is the half width at half maximum (HWHM) of the assumed mode function.

In the case of a cavity which is resonant with the zero-phonon line, we find for the integrated ZPL,

$$\mathscr{I}_{1s}^{\mathrm{ZPL}}(\eta) = \frac{\mathcal{E}_0\eta\Delta N_{1s,\mathbf{0}}}{\eta^2 + \gamma_0\eta + \mathcal{G}^2} \to \frac{\mathcal{E}_0\eta}{\mathcal{G}^2}\Delta N_{1s,\mathbf{0}}. \quad (56)$$

This is linearly proportional to the cavity η. The overall NMC PL decreases for enhanced cavity in the $1s$-cavity case.

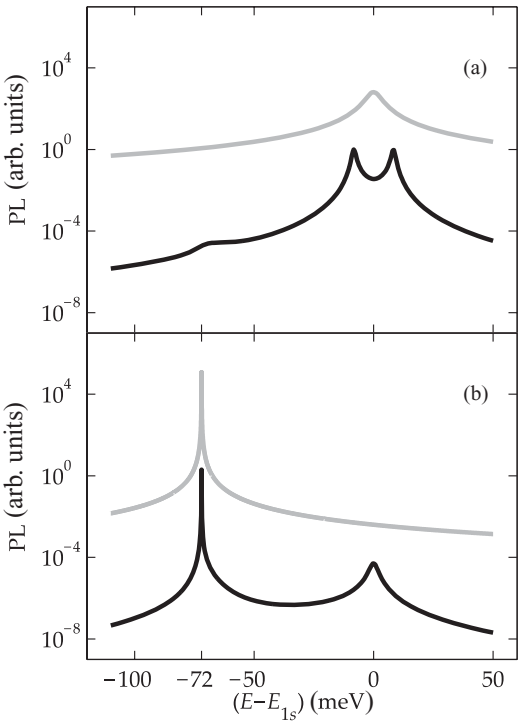

FIG. 5. Microcavity luminescence (black solid line) including the zero-phonon line (ZPL) and the first phonon sideband (PSB_1) calculated via the analytic model. The cavity is resonant with (a) the ZPL or (b) the PSB_1. The corresponding mode function is shown by the gray solid line.

For the phonon cavity, the first sideband PL integrates to

$$\mathscr{I}_{\mathrm{ph}}^{\mathrm{PSB}}(\eta) = \sum_{\mathbf{p}}\frac{\mathcal{E}_0\chi_{\mathbf{p}}[\Delta E_{\mathbf{p}}(\gamma_0 + \eta) + (\gamma_1 + \eta)\hbar\Omega]}{[(\Delta E_{\mathbf{p}})^2 + (\gamma_1 + \eta)^2][(\gamma_0 + \eta)^2 + \hbar^2\Omega^2]}, \quad (57)$$

where $\Delta E_{\mathbf{p}} \equiv E_{1s,\mathbf{p}} - E_{1s,\mathbf{0}}$. In the limit of $\eta \to 0$, we find for Eq. (57) that

$$\lim_{\eta\to 0}\mathscr{I}_{\mathrm{ph}}^{\mathrm{PSB}}(\eta) = \sum_{\mathbf{p}}\frac{\mathcal{E}_0\chi_{\mathbf{p}}[\Delta E_{\mathbf{p}}\,\gamma_0 + \gamma_1\hbar\Omega]}{[(\Delta E_{\mathbf{p}})^2 + \gamma_1^2]\hbar^2\Omega^2} \quad (58)$$

saturates to a constant level, unlike Eq. (56). In other words, Eqs. (56) and (58) confirm the numerical result in Fig. 6 that the cavity changes the exciton and the phonon resonance differently when it is tuned into the respective resonances.

To graphically illustrate the analytic result (44), we present in Fig. 5 the corresponding PL spectra for the $1s$ cavity and the phonon cavity. The black solid lines show the PL spectra and the gray solid lines show the corresponding mode function used in the calculation. We see that the results are qualitatively very similar to the full numerical analysis in Fig. 4. In particular, the $1s$ cavity produces a splitting of the PL resonances, whereas the phonon cavity enhances the PL at the sideband.

The analytic model can also be applied to derive the integrated spectra shown in Fig. 6. The yellow solid line represents the intensity of the ZPL photoluminescence using the $1s$ cavity, and the black solid line shows the PSB_1 photoluminescence for the phonon cavity. We see again that

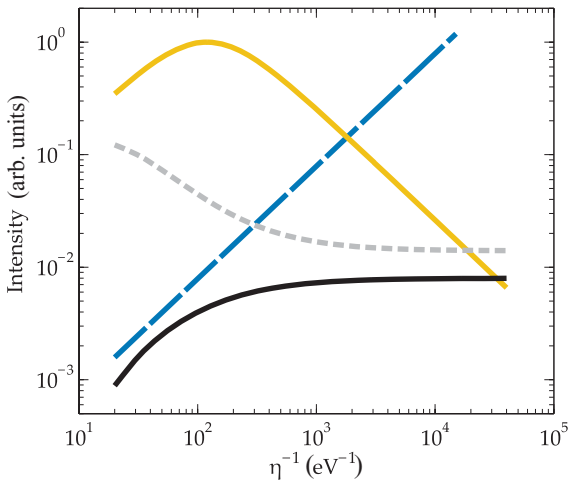

FIG. 6. (Color online) Intensity of the photoluminescence spectrum calculated with the analytic model. The yellow (gray) solid line shows the intensity of the exciton resonance using 1*s* cavity, whereas the intensity of the phonon peak with phonon cavity is represented by the black solid line. The short-dashed line (black) is the total intensity with phonon cavity. The mode function maximum is shown by the long-dashed line (blue). The top x axis indicates the number of DBR mirror pairs which correspond to the mode-function HWHM at the bottom x axis.

the ZPL intensity first increases but then starts decreasing at the point when the exciton resonance splits due to the transition into the nonperturbative regime. The saturation of the PSB_1 intensity for the narrow mode function shown by the black solid line can clearly be seen. The dashed gray line depicts the complete PL intensity using the phonon cavity, showing again that for a high reflectivity, the PSB_1 PL obviously dominates the system. The long-dashed blue line indicates an exponential increase of the mode function maximum. The x axis on the top of the figure shows the appropriate numbers of DBR mirror pairs, as used in the numerical studies, which correspond to the mode function's linewidth η on the bottom x axis.

VI. CONCLUSIONS

In this work, we have presented a microscopic many-body theory to describe phonon-assisted luminescence in a microcavity. In addition to a full numerical evaluation of the phonon-assisted semiconductor luminescence equations, we developed a rigorous analytic model. By introducing the strong-cavity approximation, we are able to find a consistent way to handle the stimulated parts in the semiconductor luminescence equations and formulate a closed analytical formula for the cavity PL. We find that the phonon-sideband luminescence is strongly enhanced if the cavity resonance is shifted to coincide with the first phonon-sideband resonance. With the help of the analytic model, it could be shown that the PL intensity first increases due to the Purcell effect, but then starts decreasing due to the transition into the nonperturbative regime if the cavity is resonant with the zero-phonon line. For a cavity that is resonant with the phonon sideband, the integrated PL saturates, which indicates a qualitative change in the cavity effects.

ACKNOWLEDGMENTS

This work is supported by the Deutsche Forschungsgemeinschaft. In particular, C.B. wants to thank the International Research Training Group 790 *Electron–Electron Interactions in Solids* (Marburg-Budapest) for financial support.

APPENDIX A: EXCITON BASIS

In this work, a generalized exciton basis is used to solve the analytic model as well as Eq. (14). We write the general exciton state ν as

$$|X_{\nu,\mathbf{Q}}\rangle = \sum_{\mathbf{k}} \phi_{\nu}(\mathbf{k})\, a^{\dagger}_{\mathrm{c},\,\mathbf{k}+\mathbf{Q}_\mathrm{e}} a_{\mathrm{v},\,\mathbf{k}-\mathbf{Q}_\mathrm{h}} |\mathrm{G}\rangle, \tag{A1}$$

where we introduced the center-of-mass momenta $\mathbf{Q}_{\{\mathrm{e,h}\}} = \frac{m_{\{\mathrm{e,h}\}}}{M}\mathbf{Q}$ and the total mass $M = m_\mathrm{e} + m_\mathrm{h}$ of an electron–hole pair, while the ground state of a semiconductor is characterized by a completely filled valence band and an empty conduction band via $|\mathrm{G}\rangle = \Pi_{\mathbf{k}} a^{\dagger}_{\mathrm{v},\,\mathbf{k}} |\mathrm{vac}\rangle$. By minimizing the energy of the carrier system in the low-density regime, the variational principle leads to a Hermitian eigenvalue problem for the *excitonic wave function* $\phi_\nu(\mathbf{k})$, which is represented by the so-called Wannier equation,

$$E_{\nu,\mathbf{Q}}\phi_{\nu}(\mathbf{k}) = \left(\varepsilon^{\mathrm{e}}_{\mathbf{k}+\mathbf{Q}_\mathrm{e}} + \varepsilon^{\mathrm{h}}_{\mathbf{k}-\mathbf{Q}_\mathrm{h}}\right)\phi_{\nu}(\mathbf{k}) - \sum_{\mathbf{k}'} V_{\mathbf{k}-\mathbf{k}'}\phi_{\nu}(\mathbf{k}'). \tag{A2}$$

Here, $E_{\nu,\mathbf{Q}} = \mathcal{E}_\nu + \frac{\hbar^2\mathbf{Q}^2}{2M}$ decomposes into the excitonic eigenenergy $\mathcal{E}_\nu$ and the center-of-mass energy of the electron–hole pair. A Fourier transformation into real space leads to the equation of the relative motion of the hydrogen atom. Since the problem is Hermitian, the eigenfunctions build a complete set of orthogonalized functions, which can be used to expand the linearized semiconductor Bloch equations to obtain an Elliott formula as an analytic result.

In the case of nonvanishing densities, the problem becomes non-Hermitian and it is helpful to introduce left- and right-handed eigenfunctions that solve the *excitonic eigenvalue equations*,

$$\begin{aligned} E_{\nu,\mathbf{Q}}\phi^{\mathrm{R}}_{\nu,\mathbf{Q}}(\mathbf{k}) = {} & \left(\tilde{\varepsilon}^{\mathrm{e}}_{\mathbf{k}+\mathbf{Q}_\mathrm{e}} + \tilde{\varepsilon}^{\mathrm{h}}_{\mathbf{k}-\mathbf{Q}_\mathrm{h}}\right)\phi^{\mathrm{R}}_{\nu,\mathbf{Q}}(\mathbf{k}) \\ & - \left(1 - f^{\mathrm{e}}_{\mathbf{k}+\mathbf{Q}_\mathrm{e}} - f^{\mathrm{h}}_{\mathbf{k}-\mathbf{Q}_\mathrm{h}}\right)\sum_{\mathbf{k}'} V_{\mathbf{k}-\mathbf{k}'}\phi^{\mathrm{R}}_{\nu,\mathbf{Q}}(\mathbf{k}'), \end{aligned} \tag{A3}$$

$$\begin{aligned} \left[\phi^{\mathrm{L}}_{\nu,\mathbf{Q}}(\mathbf{k})\right]^{\star} E_{\nu,\mathbf{Q}} = {} & \left[\phi^{\mathrm{L}}_{\nu,\mathbf{Q}}(\mathbf{k})\right]^{\star}\left(\tilde{\varepsilon}^{\mathrm{e}}_{\mathbf{k}+\mathbf{Q}_\mathrm{e}} + \tilde{\varepsilon}^{\mathrm{h}}_{\mathbf{k}-\mathbf{Q}_\mathrm{h}}\right) \\ & - \sum_{\mathbf{k}'}\left(1 - f^{\mathrm{e}}_{\mathbf{k}'+\mathbf{Q}_\mathrm{e}} - f^{\mathrm{h}}_{\mathbf{k}'-\mathbf{Q}_\mathrm{h}}\right) V_{\mathbf{k}-\mathbf{k}'}\phi^{\mathrm{L}}_{\nu,\mathbf{Q}}(\mathbf{k}'). \end{aligned} \tag{A4}$$

These eigenfunctions obey the *generalized orthogonality and completeness relations*

$$\sum_{\mathbf{k}} \left[\phi^{\mathrm{L}}_{\nu,\mathbf{Q}}(\mathbf{k})\right]^{\star}\phi^{\mathrm{R}}_{\nu',\mathbf{Q}}(\mathbf{k}) = \delta_{\nu,\nu'}, \tag{A5a}$$

$$\sum_{\nu} \left[\phi^{\mathrm{L}}_{\nu,\mathbf{Q}}(\mathbf{k})\right]^{\star}\phi^{\mathrm{R}}_{\nu,\mathbf{Q}}(\mathbf{k}') = \delta_{\mathbf{k},\mathbf{k}'}. \tag{A5b}$$

With this, one can define the *excitonic creation and annihilation operators*

$$X^{\dagger}_{\nu,\mathbf{Q}} = \sum_{\mathbf{k}} \phi^{\mathrm{L}}_{\nu,\mathbf{Q}}(\mathbf{k}) a^{\dagger}_{\mathrm{c},\mathbf{k}+\mathbf{Q}_\mathrm{e}} a_{\mathrm{v},\mathbf{k}-\mathbf{Q}_\mathrm{h}}, \tag{A6a}$$

$$X_{\nu,\mathbf{Q}} = \sum_{\mathbf{k}} \left[\phi^{\mathrm{L}}_{\nu,\mathbf{Q}}(\mathbf{k})\right]^{\star} a^{\dagger}_{\mathrm{v},\mathbf{k}-\mathbf{Q}_\mathrm{h}} a_{\mathrm{c},\mathbf{k}+\mathbf{Q}_\mathrm{e}}, \tag{A6b}$$

which can be inverted back to the single-particle basis via

$$a^{\dagger}_{\mathrm{c},\mathbf{k}+\mathbf{Q}_\mathrm{e}} a_{\mathrm{v},\mathbf{k}-\mathbf{Q}_\mathrm{h}} = \sum_{\nu} \left[\phi^{\mathrm{R}}_{\nu,\mathbf{Q}}(\mathbf{k})\right]^{\star} X^{\dagger}_{\nu,\mathbf{Q}}, \tag{A7a}$$

$$a^{\dagger}_{\mathrm{v},\mathbf{k}-\mathbf{Q}_\mathrm{h}} a_{\mathrm{c},\mathbf{k}+\mathbf{Q}_\mathrm{e}} = \sum_{\nu} \phi^{\mathrm{R}}_{\nu,\mathbf{Q}}(\mathbf{k})\ X_{\nu,\mathbf{Q}}. \tag{A7b}$$

In the low-density regime, it is justified to replace $\phi^{\{\mathrm{L},\mathrm{R}\}}_{\nu,\mathbf{Q}}(\mathbf{k})$ by $\phi_{\nu}(\mathbf{k})$.

APPENDIX B: ANALYTICAL MODEL

Applying the definitions (24)–(26b), (32), and (33), and the strong-cavity approximation introduced in Eq. (29), to Eqs. (20) and (21), we eventually compute the dynamic equations

$$\begin{aligned}
&\mathrm{i}\hbar\frac{\partial}{\partial t}\begin{pmatrix} \Delta\langle \bar{D}^{\dagger}_{\mathbf{p},\Sigma}\bar{B}^{\dagger}_{\mathbf{0},q_\perp}X_{\mathbf{p}}\rangle \\ \Delta\langle \bar{D}^{\dagger}_{\mathbf{0},\Sigma}\bar{B}^{\dagger}_{\mathbf{0},q_\perp}\bar{B}^{\dagger}_{\mathbf{0},\Sigma}\rangle \end{pmatrix} \\
&= \begin{pmatrix} \Delta^{\mathrm{PSB},-}_{\omega,\mathbf{p}} - \mathrm{i}\gamma_1 & -\mathrm{i}\mathcal{G}\delta_{\mathbf{p},\mathbf{0}} \\ \mathrm{i}\mathcal{G} & \Delta^{\mathrm{cav}}_{\omega} - \hbar\Omega \end{pmatrix} \cdot \begin{pmatrix} \Delta\langle \bar{D}^{\dagger}_{\mathbf{p},\Sigma}\bar{B}^{\dagger}_{\mathbf{0},q_\perp}X_{\mathbf{p}}\rangle \\ \Delta\langle \bar{D}^{\dagger}_{\mathbf{0},\Sigma}\bar{B}^{\dagger}_{\mathbf{0},q_\perp}\bar{B}^{\dagger}_{\mathbf{0},\Sigma}\rangle \end{pmatrix} \\
&\quad + \mathrm{i}\begin{pmatrix} \chi_{\mathbf{p}} \\ \Delta\langle \bar{D}^{\dagger}_{\mathbf{0},\Sigma}\bar{B}_{\mathbf{0},\Sigma}X^{\dagger}_{\mathbf{0}}\rangle \end{pmatrix}.
\end{aligned} \tag{B1}$$

Even though Eqs. (35) and (B1) have a much simpler format than the original equations, they still contain unknown collective contributions on the right-hand side. To solve these, we need to additionally evaluate

$$\begin{aligned}
&\mathrm{i}\hbar\frac{\partial}{\partial t}\Delta\langle \bar{D}^{\dagger}_{\mathbf{0},\Sigma}\bar{B}^{\dagger}_{\mathbf{0},\Sigma}\bar{B}_{\mathbf{0},\Sigma}\rangle \\
&= -\hbar\Omega\Delta\langle \bar{D}^{\dagger}_{\mathbf{0},\Sigma}\bar{B}^{\dagger}_{\mathbf{0},\Sigma}\bar{B}_{\mathbf{0},\Sigma}\rangle \\
&\quad + \mathrm{i}\,\mathcal{G}(\Delta\langle \bar{D}^{\dagger}_{\mathbf{0},\Sigma}\bar{B}_{\mathbf{0},\Sigma}X^{\dagger}_{\mathbf{0}}\rangle + \Delta\langle \bar{D}^{\dagger}_{\mathbf{0},\Sigma}\bar{B}^{\dagger}_{\mathbf{0},\Sigma}X_{\mathbf{0}}\rangle),
\end{aligned} \tag{B2}$$

$$\begin{aligned}
&\mathrm{i}\hbar\frac{\partial}{\partial t}\Delta\langle \bar{D}^{\dagger}_{\mathbf{0},\Sigma}\bar{B}_{\mathbf{0},\Sigma}X^{\dagger}_{\mathbf{0}}\rangle \\
&= [-E_{1s,\mathbf{0}} + \hbar\omega_{\mathrm{cav}} - \hbar\Omega - \mathrm{i}\gamma_1]\Delta\langle \bar{D}^{\dagger}_{\mathbf{0},\Sigma}\bar{B}_{\mathbf{0},\Sigma}X^{\dagger}_{\mathbf{0}}\rangle \\
&\quad + \mathrm{i}\,\mathcal{G}(\chi_{\mathbf{0}} - \Delta\langle \bar{D}^{\dagger}_{\mathbf{0},\Sigma}\bar{B}^{\dagger}_{\mathbf{0},\Sigma}\bar{B}_{\mathbf{0},\Sigma}\rangle),
\end{aligned} \tag{B3}$$

$$\begin{aligned}
&\mathrm{i}\hbar\frac{\partial}{\partial t}\Delta\langle \bar{D}^{\dagger}_{\mathbf{0},\Sigma}\bar{B}^{\dagger}_{\mathbf{0},\Sigma}X_{\mathbf{0}}\rangle \\
&= [E_{1s,\mathbf{0}} - \hbar\omega_{\mathrm{cav}} - \hbar\Omega - \mathrm{i}\gamma_1]\Delta\langle \bar{D}^{\dagger}_{\mathbf{0},\Sigma}\bar{B}^{\dagger}_{\mathbf{0},\Sigma}X_{\mathbf{0}}\rangle \\
&\quad + \mathrm{i}\,\mathcal{G}(\chi_{\mathbf{0}} - \Delta\langle \bar{D}^{\dagger}_{\mathbf{0},\Sigma}\bar{B}^{\dagger}_{\mathbf{0},\Sigma}\bar{B}_{\mathbf{0},\Sigma}\rangle),
\end{aligned} \tag{B4}$$

which are linear equations with damping and source terms that evolve into a steady state.

*christoph.boettge@physik.uni-marburg.de

[1] D. G. Thomas, J. Phys. Chem. Solids **15**, 86 (1960).
[2] A. Ashrafi and C. Jagadish, J. Appl. Phys. **102**, 071101 (2007).
[3] C. F. Klingshirn, Chem. Phys. Chem. **8**, 782 (2007).
[4] H. Morkoç and Ü. Özgür, *Zinc Oxide: Fundamentals, Materials and Device Technology*, 1st ed. (Wiley-VCH Verlag, Weinheim, 2009).
[5] B. K. Meyer, H. Alves, D. M. Hofmann, W. Kriegseis, D. Forster, F. Bertram, J. Christen, A. Hoffmann, M. Straßburg, M. Dworzak, U. Haboeck, and A. V. Rodina, Phys. Status Solidi B **241**, 231 (2004).
[6] U. Ozgur, Y. I. Alivov, C. Liu, A. Teke, M. A. Reshchikov, S. Dogan, V. Avrutin, S.-J. Cho, and H. Morkoc, J. Appl. Phys. **98**, 041301 (2005).
[7] Y. Segawa, H. Sun, T. Makino, M. Kawasaki, and H. Koinuma, Phys. Status Solidi A **192**, 14 (2002).
[8] W. Shan, W. Walukiewicz, J. W. Ager III, K. M. Yu, H. B. Yuan, H. P. Xin, G. Cantwell, and J. J. Song, Appl. Phys. Lett. **86**, 191911 (2005).
[9] W. Y. Liang and A. D. Yoffe, Phys. Rev. Lett. **20**, 59 (1968).
[10] S. J. Xu, S.-J. Xiong, and S. L. Shi, J. Chem. Phys. **123**, 221105 (2005).
[11] T. Feldtmann, M. Kira, and S. W. Koch, Phys. Status Solidi B **246**, 332 (2009).
[12] C. F. Klingshirn, Phys. Status Solidi B **202**, 1521 (1997).
[13] L. Li, H. Yang, G. Qi, J. Ma, X. Xie, H. Zhao, and F. Gao, Chem. Phys. Lett. **455**, 93 (2008).
[14] S. Ramanathan, S. Bandyopadhyay, L. K. Hussey, and M. Munoz, Appl. Phys. Lett. **89**, 143121 (2006).
[15] H. Zhao, S. Moehl, and H. Kalt, Appl. Phys. Lett. **81**, 2794 (2002).
[16] R. Kuhnert and R. Helbig, J. Lumin. **26**, 203 (1981).
[17] T. Feldtmann, M. Kira, and S. W. Koch, J. Lumin. **130**, 107 (2010).
[18] X. B. Zhang, T. Taliercio, S. Kolliakos, and P. Lefebvre, J. Phys. Condens. Matter **13**, 7053 (2001).
[19] M. Kozhevnikov, B. M. Ashkinadze, E. Cohen, and A. Ron, Solid State Commun. **106**, 73 (1998).
[20] M. Soltani, M. Certier, R. Evrard, and E. Kartheuser, J. Appl. Phys. **78**, 5626 (1995).
[21] L. T. Tan, R. W. Martin, K. P. O'Donnell, and I. M. Watson, Appl. Phys. Lett. **89**, 101910 (2006).
[22] E. M. Purcell, Phys. Rev. **69**, 681 (1946).
[23] E. Yablonovitch, Phys. Rev. Lett. **58**, 2059 (1987).
[24] C. Weisbuch, M. Nishioka, A. Ishikawa, and Y. Arakawa, Phys. Rev. Lett. **69**, 3314 (1992).
[25] G. Khitrova, H. M. Gibbs, F. Jahnke, M. Kira, and S. W. Koch, Rev. Mod. Phys. **71**, 1591 (1999).
[26] F. Jahnke, M. Kira, S. W. Koch, G. Khitrova, E. K. Lindmark, T. R. Nelson Jr., D. V. Wick, J. D. Berger, O. Lyngnes, H. M. Gibbs, and K. Tai, Phys. Rev. Lett. **77**, 5257 (1996).

[27]M. Kira, F. Jahnke, W. Hoyer, and S. W. Koch, Prog. Quantum Electron. **23**, 189 (1999).
[28]M. Kira, F. Jahnke, and S. W. Koch, Phys. Rev. Lett. **81**, 3263 (1998).
[29]M. Kira and S. W. Koch, Prog. Quantum Electron. **30**, 155 (2006).
[30]H. Haug and S. W. Koch, *Quantum Theory of the Optical and Electronic Properties of Semiconductors*, 5th ed. (World Scientific, Singapore, 2009).
[31]M. Kira and S. W. Koch, Phys. Rev. A **78**, 022102 (2008).
[32]J. Čížek, J. Chem. Phys. **45**, 4256 (1966).
[33]G. D. Purvis III and R. J. Bartlett, J. Chem. Phys. **76**, 1910 (1982).
[34]J. Fricke, Ann. Phys. (NY) **252**, 479 (1996).
[35]H. W. Wyld Jr. and B. D. Fried, Ann. Phys. (NY) **23**, 374 (1963).
[36]T. Feldtmann, Ph.D. thesis, Fachbereich Physik, Philipps-Universität Marburg, 2009.
[37]H. Fröhlich, Adv. Phys. **3**, 325 (1954).
[38]H. Fröhlich, Proc. R. Soc. London **215**, 291 (1952).
[39]H. Haken, *Quantenfeldtheorie des Festkörpers* (Teubner, Stuttgart, 1973).
[40]I. V. Bondarev, S. A. Maksimenko, G. Y. Slepyan, I. L. Krestnikov, and A. Hoffmann, Phys. Rev. B **68**, 073310 (2003).
[41]D. Braun, W. W. Rühle, C. Trallero-Giner, and J. Collet, Phys. Rev. Lett. **67**, 2335 (1991).
[42]W. A. Harrison, Phys. Rev. **104**, 1281 (1956).
[43]G. Coli and K. K. Bajaj, Appl. Phys. Lett. **78**, 2861 (2001).
[44]C. F. Klingshirn, Phys. Status Solidi B **244**, 3027 (2007).
[45]A. A. Serdobintsev, E. I. Burylin, A. G. Veselov, O. A. Kiryasova, and A. S. Dzhumaliev, Tech. Phys. **53**, 368 (2008).
[46]C. W. Teng, J. F. Muth, Ü. Özgür, M. J. Bergmann, H. O. Everitt, A. K. Sharma, C. Jin, and J. Narayan, Appl. Phys. Lett. **76**, 979 (2000).
[47]N. B. Chen, H. Z. Wu, D. J. Qiu, T. N. Xu, J. Chen, and W. Z. Shen, J. Phys. Condens. Matter **16**, 2973 (2004).
[48]R. Schmidt, B. Rheinländer, M. Schubert, D. Spemann, T. Butz, J. Lenzner, E. M. Kaidashev, M. Lorenz, A. Rahm, H. C. Semmelhack, and M. Grundmann, Appl. Phys. Lett. **82**, 2260 (2003).
[49]W. von Sellmeier, Ann. Phys. (Leipzig) **143**, 272 (1871).
[50]S. Chatterjee, C. Ell, S. Mosor, G. Khitrova, H. M. Gibbs, W. Hoyer, M. Kira, S. W. Koch, J. P. Prineas, and H. Stolz, Phys. Rev. Lett. **92**, 067402 (2004).